How to cite: Marques, R., Pereira, J. M., Lourenço, P. B. (2020). Lateral in-plane seismic response of confined masonry walls: From numerical to backbone models. Engineering Structures, 221, 111098. doi:10.1016/j.engstruct.2020.111098

Lateral in-plane seismic response of confined masonry walls: from numerical to backbone models

Rui Marques*, João M. Pereira, Paulo B. Lourenço

ISISE, Institute of Science and Innovation for Bio-Sustainability (IB-S), University of Minho, Guimarães, Portugal

* Address correspondence to Rui Marques, Department of Civil Engineering, University of Minho, Campus de Azurém, 4800-058 Guimarães, Portugal; E-mail: marquesmnc@sapo.pt

Abstract: Confined masonry (CM) is a widely used solution for buildings in developing countries and has potential for worldwide application when considering its economic and constructive advantages. Although a large background of experimental testing of CM walls is available, numerical studies are further needed to extend the existing knowledge and derive analytical rules to adopt in design codes. In this work, a parametric numerical study is performed, aimed to characterize the lateral in-plane response of CM walls under different variables and to establish a dataset for comparison of engineering demand parameters, towards the proposal of predictive models. Benchmark walls tested under lateral in-plane loading are used to calibrate a finite element modelling approach for pushover analysis. Based on the results of the parametric study, a formulation and charts are proposed to respectively estimate the lateral resistance and displacement capacity of CM walls with features similar to the ones used as benchmark.

Keywords: confined masonry, numerical modelling, pushover analysis, resistance criteria, drift estimation charts, backbone models

1. Introduction

Confined masonry (CM) construction, i.e. unreinforced masonry (URM) panels usually strengthened with reinforced concrete (RC) tie-elements, has been largely used in Latin America. Furthermore, its application has widespread worldwide, particularly in developing countries, like Algeria and Iran. Many of the CM buildings are non-engineered structures, i.e. no structural analysis and safety check are carried out for their design, mainly because of limited local resources and lack of an effective management and control policy in the building sector. The dissemination of CM towards a more efficient application requires a better understanding of its structural behaviour, far beyond extensive experimental testing.

CM buildings are composed of masonry walls which are enclosed by RC confining elements in both vertical (tie-column) and horizontal (tie-beam) directions, so that all materials act compositely in resisting action effects. CM structures are similar to RC infilled frames, with the main difference that in CM the frame elements in concrete are cast only after the masonry walls are built, so that in CM there is an effective contact between masonry and the surrounding RC elements due to adhesion and confinement effects.

A wide knowledge concerning the experimental response of CM walls subjected to lateral in-plane loading has been mostly established in Latin America, although it has also resulted in dispersion of rules in design codes; see Meli et al. (2011) [1]. Furthermore, research on CM structures has been based on the assumption that the wall in-plane response is dominated by diagonal shear, even for slender walls, e.g. Pérez-Gavilán et al. (2015) [2]. Indeed, the assumed diagonal shear failure of CM walls has biased the design of CM walls, so that the prescriptions given in design codes always induce a shear-dominated behaviour. Varela-Rivera et al. (2019) [3] have studied the flexural behaviour of CM walls and they advocate reducing the amount of steel reinforcement in tie-columns to induce flexural behaviour rather than shear behaviour, since the flexural failure is more ductile.

There are however different variables which can influence the behaviour of CM walls subjected to lateral in-plane loads, beyond the amount of steel reinforcement in tie-columns, namely the wall aspect ratio (height to length ratio), the vertical stress on the wall, the tie-column cross-section, as well as the masonry quality. Moreover, the behaviour of CM walls is rather complex since it involves a multipart interaction between the masonry panel and the confinements through a common interface. Modelling this interface adds in complexity, because it strongly influences the stress distribution between the masonry panel and the tie-elements, increases the number of parameters to consider and makes computational convergence more difficult. So, the challenge in using computational methods and applied numerical analysis to study the complex behaviour of CM walls is launched.

Performing numerical simulation allows to consider a large number of variables with avoiding the monetary cost and uncertainty associated to experimental testing. Furthermore, the combined shear-flexural mechanism of CM walls is difficult to discern in experimental testing, while numerical simulation can provide with well-monitored results to understand the compound mechanism. The effect of the wall aspect ratio on the shear-flexural interaction mechanism is an important aspect to consider, since currently there is no agreement on how it can influence the wall lateral response, and even different theories have been proposed [4].

The investigation of the deformation characteristics of CM walls is another topic to address in order to define suitable backbone models for the lateral force–displacement response, towards the application of performance-based seismic design. So, the computational approach requires also to consider the yielding stage of the walls. The extraction of useful knowledge and feasible rules from the computations is another challenge to face, since it requires the derivation of comprehensive analytical formulations from raw numerical results, and further satisfying the compromise of proposing easy-to-use methods to include in design codes. To this end, the proposed analytical rules should preferably be based on mechanical models rather than empirical formulas.

The first purpose of this work is to idealize and perform a parametric study of CM walls subjected to lateral in-plane loading, through finite element modelling and pushover analysis, including calibration of the computational approach against the results of a benchmark experimental program. The study aims to compare the lateral in-plane behaviour of CM walls when varying different variables, namely the wall aspect ratio, the vertical load, the tie-column cross-section and the amount of longitudinal reinforcement in tie-columns. Then, it will be possible to assess the effect of each variable on the lateral in-plane response of the walls, in terms of stiffness, resistance, strain and stress patterns, and drift capacity. Finally, a formulation for the lateral resistance, charts to estimate the drift ratio, as well as backbone models for the force–drift response of CM walls, are proposed based on the obtained numerical results.

2. Background studies

Most of studies on CM are based on experimental testing of walls subjected to lateral in-plane loading. A review on the structural behaviour of CM walls is presented in Marques and Lourenço (2019) [4] based on a collection of results from experimental tests in the literature. Numerical modelling of CM walls is a less studied topic, although it is important, both in research to complement and extend the experimental results when the walls are subjected to different conditions, and in design to derive suitable calculation models. A parametric study through numerical simulation of CM walls was developed by Janaraj and Dhanasekar (2015) [5] in order to propose a design expression for the in-plane shear capacity of CM shear walls containing squat panels.

More recently, Tripathy and Singhal (2019) [6] performed a parametric analysis based on a large set of finite element models, intended to realize the behaviour of the masonry strut and to develop a formulation for the strut-and-tie model in CM walls. The work presented here is also based on a parametric numerical study, but it intends to go further in discussing the parameters for a lateral force–displacement backbone model. In the following, a review of numerical modelling approaches for CM walls is made, and afterwards a benchmark experimental program carried out by Zabala et al. (2004) [7] is presented, whose results will be later used as reference for calibration of the numerical model.

2.1 Numerical modelling approaches

As pointed before, numerical simulation of CM walls is a less studied topic. There is some background on the topic of infill walls which has been adopted for the case of CM walls, e.g. Tomaževič (1999) [8]. For instance, Uva et al. (2012) [9] proposed a model for infilled frames in which the nonlinear behaviour of RC beams and columns is modelled by introducing plastic (shear and flexural) hinges at the element-ends. To account for the stiffening effect of the masonry infill, multiple diagonal struts are connected among the beam-column joints. So, in this case, the interaction between the masonry panel and the confinements is simulated only at the wall corners.

The modelling of a CM wall requires however the contact between beams/columns and masonry to be simulated along the entire interface, needing the insertion of a significant number of struts. Moreover, the consideration of the masonry panel as the main resisting part of the wall requires a more complex model to simulate the developed shear mechanism. These models, illustrated in Figure 1a-b based on the damage pattern of a wall tested under lateral cyclic loading by Pari (2008) [10], are however difficult to implement computationally. Contrarily, the macro-element proposed by Caliò et al. (2012)

[11] includes a discrete modelling of the confinement-masonry interface. Beyond orthogonal and diagonal springs to respectively simulate the flexural and shear behaviours of the masonry panel, the macro-element allows to assemble beam elements (with lumped plasticity) around the border of the masonry element, through nonlinear spring interface elements, analogously to a CM wall (Fig. 1c).

Some studies can be found in the literature in which CM walls are modelled using the finite element method (FEM). Calderini et al. (2008) [12] used FEM to perform numerical analysis for a parametric study on the seismic behaviour of CM walls, with reference to an experimental test from the literature. They adopted nonlinear constitutive laws for masonry and concrete. For masonry, a constitutive model which considers both frictional and cohesive strength components of masonry, on the basis of a micromechanical approach of the composite continuum, was used. The masonry panel and concrete tie-elements were modelled using 3-node plane stress elements. Steel reinforcements were simulated by means of linear truss elements. The adherence (interface) between masonry and concrete was modelled by using a joint of limited thickness between the two materials.

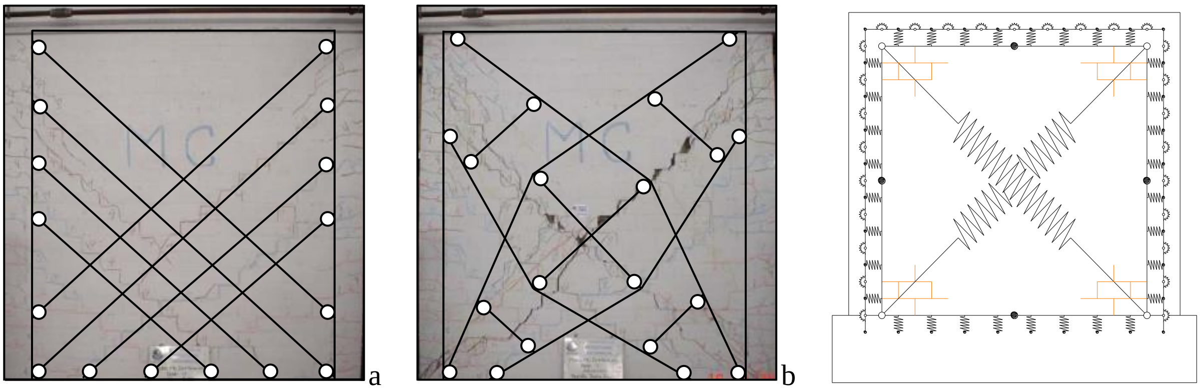

a b c

Figure 1. Models for CM walls with (a) multiple struts and (b) trusses and ties based on damage pattern of wall tested by Pari (2008) [10], and (c) assemblage of discrete springs by Caliò et al. (2012) [11]

Ranjbaran et al. (2012) [13] performed numerical analysis of CM walls to derive simple analytical formulas for seismic assessment. In this case, for modelling the masonry panels, a continuum finite element model was used in a homogenized medium, and Rankine and Hill type criteria were assumed for the inelastic behaviour in tension and compression, respectively. In these models, orthotropic behaviour was taken into account, and a combined crack-shear-crush model was used. Beam elements with moment-resisting connections were adopted to model the confining elements. For concrete of tie-elements a total strain rotating crack model was used, while the longitudinal steel bars were assumed to have full bond with concrete and follow the von Mises criterion with associated perfect elastoplastic flow. For the masonry–tie-elements interaction a discrete crack model was used. Similar modelling approaches were adopted by Eshghi and Pourazin (2009) [14] and Janaraj and Dhanasekar (2014) [15].

A hybrid finite-discrete element approach has been implemented by Smoljanović et al. (2017) [16] for detailed micro-modelling of CM walls. In this case, the masonry is modelled as an assemblage of extended units connected with zero thickness interface elements. The extended units are discretized by means of triangular finite elements, while the potential cracks in the units are considered through contact elements between the finite element mesh and follow a combined single and smeared crack model. The concrete and reinforcing bars are assembled using triangular finite elements with elastic behaviour, but nonlinear behaviour of concrete in tension and shear is modelled using concrete contact elements, and nonlinear behaviour of steel bars after cracking of concrete is modelled using reinforcing contact elements. This modelling strategy is however difficult to implement and very computationally demanding, particularly for practical purposes.

A more simplified modelling approach was used by Medeiros et al. (2013) [17], which was adopted because of the limited data required. In that work, masonry and concrete were assumed to follow a similar material model, despite their different behaviours. An isotropic smeared crack model with fixed crack orientation and constant shear degradation was adopted for both materials in the nonlinear range. The model directly relates the principal stress with principal strain values, and the relation is established based on constitutive laws for the behaviour of the material in tension, compression and shear, before and after the appearance of cracks. In this case, no explicit interface was considered between masonry and concrete, although different tensile-strain relations were assumed for masonry and concrete in order to capture the interaction behaviour around the masonry-concrete connection.

An intermediate approach was implemented by Okail et al. (2016) [18], in whose work a Mohr-Coulomb strength criterion was assumed for both concrete and masonry. In this case, the interface between the masonry panel and the concrete frame was modelled as a 'hard contact' for the normal direction and as frictional in the tangential direction. This last feature was also adopted by Tripathy and Singhal (2019) [6], with tie-constraints provided to model the interaction behaviour at the masonry–tie-element interfaces to account for the slip phenomena. In this last work, the masonry was modelled at macroscopic level while the tie-elements and interaction properties were set at microscopic scale, and a damage plasticity-based model was adopted for the inelastic behaviour of masonry and concrete.

2.2 Benchmark experimental program

In this subsection, the testing program by Zabala et al. (2004) [7] is presented and the relevant results are reported, in view of the parametric study to develop through FEM simulation of the benchmark wall. They tested a set of six real scale CM walls, which were designed to be representative of three storey residential buildings constructed according to the common practice in Argentina. The walls were built using handmade solid clay bricks with dimensions of about 17.5 cm width x 26.5 cm length x 6.5 cm high, and mortar joints of around 2 cm. The confinement was provided by RC elements with a cross-section of 20 cm x 20 cm through the full thickness of the wall, since the masonry panel was finished with 1 cm mortar plaster in both faces.

The masonry was characterized through simple compression tests of brick piles and diagonal compression tests of masonry prisms, according to the Argentinean code [19], and considering three quality levels by varying the mortar mixing ratio cement:lime:sand: (1) normal strength (1:1:5), mean compressive strength of brick piles was 4.1 MPa and mean diagonal shear strength of masonry prisms was 0.22 MPa; (2) intermediate strength (1:0.5:4), mean compressive strength of brick piles was 5.0 MPa and mean diagonal shear strength of masonry prisms was 0.28 MPa; (3) high strength (1:0:3), mean compressive strength of brick piles was 8.7 MPa and mean diagonal shear strength of masonry prisms was 0.31 MPa. The mortar of the tested walls, which are later used for calibration of the numerical models, was of the type with intermediate strength. The mean compressive strength of bricks was reported with a value of 8.2 MPa and the mean elastic modulus measured in the brick piles subjected to simple compression was 1600 MPa. The nominal yield strength of steel bars was 420 MPa.

The wall dimensions and the detailing of the reinforcement of tie-elements and foundation are presented in Figure 2a. It can be noted that the spacing of stirrups was reduced at the tie-element ends in order to increase the shear strength at the wall corners. Each wall was tested under lateral cyclic loading in displacement control, with the load applied by a hydraulic actuator at the wall top, where free rotation is allowed. During testing, the vertical stress was maintained constant by applying a vertical load through a steel beam by means of two vertical servo-controlled actuators. The test setup and instrumentation of the wall are presented in Figure 2b. The number of lateral cyclic loadings was established so that damage to the wall was controlled, but in most cases two loading cycles were applied.

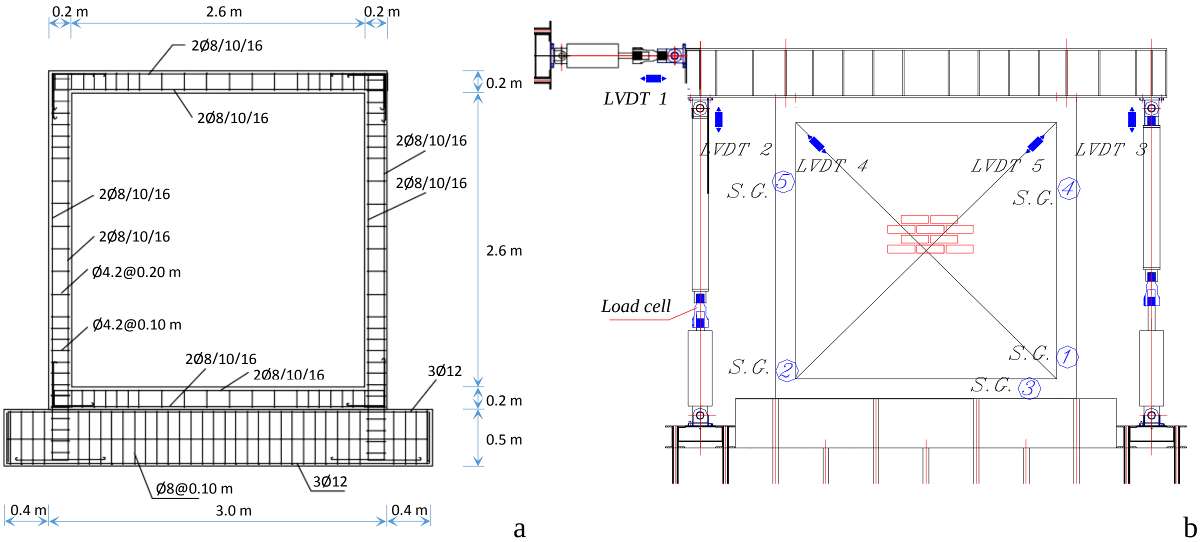

a b

Figure 2. Benchmark wall: (a) model dimensions and reinforcement details, and (b) testing apparatus (adapted from Zabala et al. (2004) [7])

The main characteristics of the tested walls are reported in Table 1. For a first set (Walls 1–4), the amount of longitudinal reinforcement in tie-columns and the vertical load on the wall were varied to assess their influence. In this case, none of the tested walls reached the theoretical flexural resistance, and the final state was controlled by the shear strength of tie-columns since the diagonal cracking of the masonry panel propagated to them. For a second set (Walls 5–6), horizontal reinforcement was added in the masonry to ensure a shear resistance larger than the flexural one. Now, horizontal cracking was induced by bending, and no separation between tie-columns and masonry panel was observed. The final state was controlled again by the shear strength of tie-columns at the joints with the confinement beams.

Table 1. Characteristics of the tested walls

Walls	Tie-column reinf.	Bedjoint reinforcement	Vertical load	Lateral resist.	Ultimate displac.
1–2	4ϕ10 (3.12 cm^2)	-	100 kN	118–93 kN	15–19 mm
3–4	4ϕ16 (8.05 cm^2)	-	200 kN	207–235 kN	20–23 mm
5–6	4ϕ8 (2.01 cm^2)	2ϕ6 @ 2 jt. (3.1 cm^2/m)	100 kN	157–169 kN	40–35 mm

Indeed, for Walls 5 and 6 with bedjoint reinforcement the diagonal cracking was restrained and the failure mechanism occurred by a mixing of bending and sliding cracks at the lower part of the wall. Although the reinforcement rate in tie-columns was reduced, both the lateral force resistance and the displacement capacity of the wall were relatively increased due to the bedjoint reinforcement; see Table 1. In the parametric study presented below, bedjoint reinforcement is not considered because it makes the behaviour of CM walls even more complex to be studied. Further experimental investigation of CM walls with bedjoint reinforcement can be found in the literature, e.g. da Porto et al. (2011) [20] and Gouveia and Lourenço (2007) [21].

The force–displacement response at each loading stage and the damage progression throughout the several stages for Wall 2 are shown in Figure 3. In the first two stages, bedjoint sliding cracks appear at the lower part of the wall; at the third stage, sliding cracks are significantly developed at the masonry panel bottom, and sliding is observed in the force–displacement response; at stage 4, a diagonal crack (disposed from the bottom-left of the wall) originates at the middle of the masonry panel and propagates into the column-beam joints, and the right tie-column presents horizontal cracks, resulting in a significant stiffness degradation of the force–displacement response; at stage 5, diagonal cracking develops also from bottom-right, while the loops of the hysteretic response are very enlarged; finally, at stage 6 the previous diagonal cracks into tie-elements are significantly aggravated and the wall presents a large displacement. The asymmetric damage pattern of the wall is denoted in the hysteretic response of the wall; since the diagonal cracks cross the tie-elements from the bottom-left of the wall, the upper formed triangle tends to rock and slide in the negative direction, as denoted in the hysteretic response.

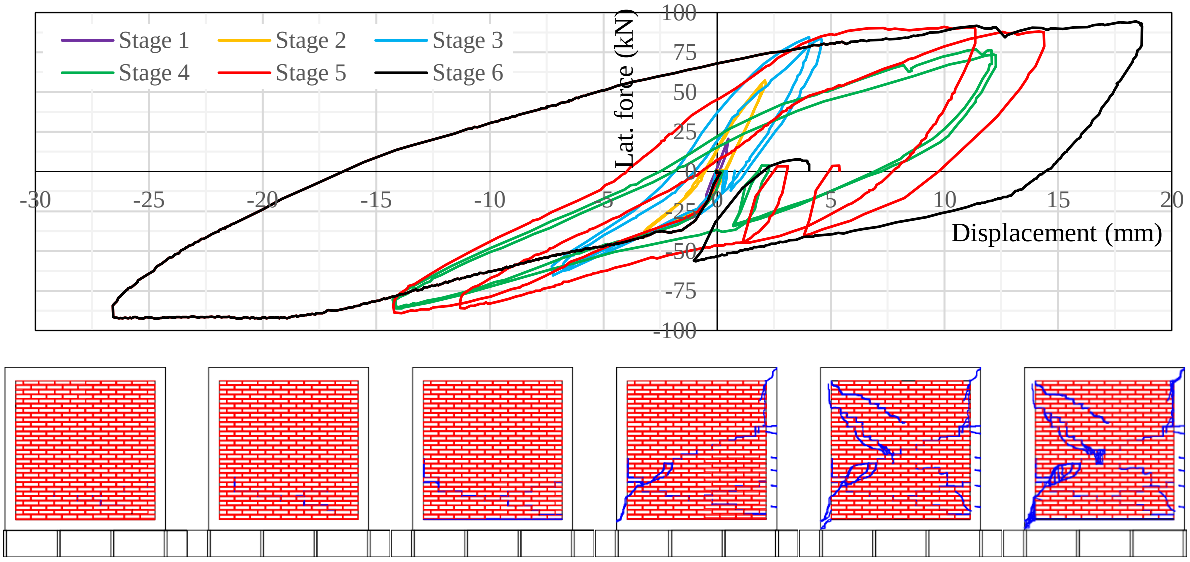

a

b

Figure 3. Shear testing of Wall 2: (a) force–displacement response at each loading stage and (b) damage progression (adapted from Zabala et al. (2004) [7])

The lateral force–displacement envelopes of the different walls are reported by Zabala et al. (2004) [7]. It was observed as there is a significant difference between them even for similar walls, due to different damage patterns driving the wall response, both in terms of lateral resistance and ultimate displacement; see Table 1. It was observed that the lateral resistance increases as the longitudinal reinforcement in tie-columns increases, while an improvement of the displacement capacity is mainly observed if bedjoint reinforcement is used. The parametric study will allow to clarify how the longitudinal reinforcement rate in tie-columns, as well as the vertical load, influence the wall response.

3. Computational modelling strategy

Advances have been verified in the development of numerical modelling approaches for masonry, both regarding the element discretization strategy and the material constitutive models. However, modelling the composite behaviour of CM is still a challenge, mainly because of the complex interaction at the frame-masonry interface. Moreover, a compromise is needed between the complexity of the model and its accuracy. The adopted strategy for numerical modelling of CM walls is described below, after that the calibration procedure of the models is reported.

3.1 Numerical approach

The computational model of the benchmark CM wall was developed in the finite element software DIANA [22], according to the geometry and mesh presented in Figure 4. The FEM models included Q8MEM four-node quadrilateral isoparametric plane stress elements to simulate the masonry and concrete sections, and L8IF (2+2 nodes) interface elements to model the frame-masonry interface. The masonry and concrete were assumed as homogenized continuum media, and a total strain crack model was adopted for them based on direct implementation of experimental observations; see Selby and

Vecchio (1993) [23]. More specifically, an isotropic smeared-crack model with rotating crack directions was adopted for both materials in the nonlinear range [22]. Indeed, the work by Rots (1988) [24] showed that for shear-dominated applications the rotating crack model results in more realistic predictions, while the fixed crack model tends to behave too stiff. The masonry and concrete were assumed to follow a similar stress-strain constitutive law, i.e. linear-exponential in tension and linear-parabolic in compression, with the compressive fracture energy G_c and the tensile fracture energy G_f^I respectively establishing the softening behaviour in compression and tension (Fig. 5a-b); see [22].

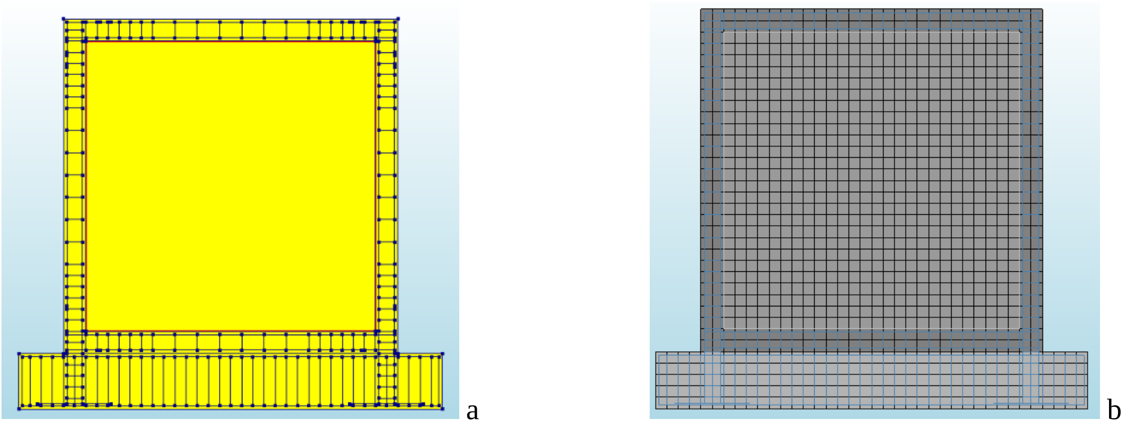

Figure 4. Computational models of the benchmark CM wall: (a) geometrical and (b) meshed

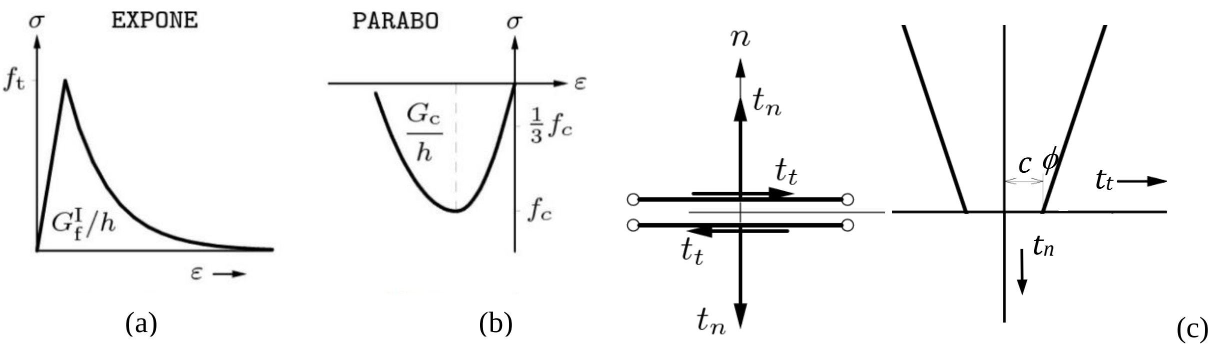

Figure 5. Material behaviour in (a) tension and (b) compression, and (c) line interface model [22]

A cohesive interface model was assumed for the frame-masonry interface (Fig. 5c). In this case, a Coulomb friction model with non-associated plasticity, i.e. yielding and plastic flow are described by two different functions, was used [22]. The mechanical parameters to consider for the interface model are: the linear stiffness modulus D_{11}, which sets the relation between the shear traction (t_t) and the shear relative displacement in the element *x*-direction; the linear stiffness modulus D_{22}, which sets the relation between the normal traction (t_n) and the normal relative displacement in the element *y*-direction; the cohesion and the friction angle at the interface; the dilatancy angle that defines the plastic volumetric strain; and eventually gap formation, i.e. if t_n exceeds a certain value it is immediately reduced to zero (brittle cracking). The longitudinal steel reinforcement and the stirrups were respectively modelled using embedded-bar and grid-reinforcement elements, while a rigid bond between the reinforcement and the concrete was assumed. The reinforcement was assumed to be an elastic–perfectly plastic material.

3.2 Calibrated models

The material properties of the concrete and steel reinforcement were assumed in the models according to specified values in design codes corresponding to the classes of strength reported by Zabala et al. (2004) [7]. Contrarily, the material properties for the masonry and interface were adjusted (by inverse fitting, iteratively changing the unknown values of mechanical parameters within suitable ranges) so that the numerical model provides a force–displacement curve globally matching the experimental response, and providing a consistent damage pattern of the walls. This procedure was performed with reference to the couples of Walls 1–2 and 3–4, to be representative of different characteristics for the walls, i.e. longitudinal reinforcement in tie-columns and vertical load, as reported below. Note that the calibration of mechanical parameters was based on the numerical simulation of monotonic lateral (push-over) loading of the benchmark CM walls, with the horizontal load applied at the tie-beam level.

The concrete of the confining elements was assumed to be of class H-17 in Argentine, with a mean compressive strength of around 20 MPa (CIRSOC-201 2005) [25]. So, for the numerical model the concrete was assumed with a compressive strength of 20 MPa, a tensile strength of 1.8 MPa and an elastic modulus of 30 GPa after correspondence of material properties in Eurocode 2 - Part 1-1 [26]. The fracture energy values were estimated based on existing codes and guidelines, e.g. fib (2013) [27]. The reinforcing steel was assumed to have a nominal yield strength of 420 MPa and an elastic modulus of 200 GPa. Any other properties needed for modelling the concrete and reinforcement were assumed according to corresponding default properties in Eurocode 2 - Part 1-1.

As reported by Zabala et al. (2004) [7], a mean masonry compressive strength of 5.0 MPa was obtained when using a mortar of the type with intermediate strength (the one used in the tested walls), from testing brick piles, while the mean elastic modulus measured in masonry prisms subjected to compression was 1600 MPa. That value of the compressive strength f_m is however hardly representative of the tested walls, because: (a) the adopted running bond originates a compressive behaviour different of the one for stack bond; (b) there is uncertainty related to the quality of the masonry materials (handmade solid clay bricks are used), even because the coefficient of variation of the masonry compressive strength may be high; and (b) the failure of the tested walls is by diagonal shear, so the masonry compressive strength in the horizontal direction plays an important role, i.e. a biaxial stress state is implied, e.g. Mojsilović (2011) [28]. Since the horizontal masonry compressive strength is usually lower than the vertical one, particularly because of the lower compressive strength of the bricks in the direction of their largest dimension, due to the fabrication process, the lateral resistance of the walls is limited by that horizontal strength. So, it was estimated for the masonry, according to the isotropic strength model used, an f_m which is about half of the vertical compressive strength.

Moreover, because of the low quality of the masonry and considering that in the tests the first cracks occurred at early loading stages (mostly at joint-brick interfaces), a 'no-tension' hypothesis was considered for the masonry, i.e. very low tensile strength (0.025 MPa) is assumed just to allow computational convergence. This low value for the masonry tensile strength was also adopted in order

How to cite: Marques, R., Pereira, J. M., Lourenço, P. B. (2020). Lateral in-plane seismic response of confined masonry walls: From numerical to backbone models. Engineering Structures, 221, 111098. doi:10.1016/j.engstruct.2020.111098

to induce a significant flexural behaviour of the CM walls. Afterwards, according to this assumption and the calibrated values for the frame-masonry interface model as reported below, the best fit to the initial stiffness of the experimental response was obtained for a masonry elastic modulus of 2000 MPa, while the best match to the experimental lateral resistance was obtained for a masonry compressive strength of 2.5 MPa (as previously estimated). The compressive and tensile fracture energies were estimated based on the corresponding strengths, according to Angelillo et al. (2014) [29].

For the frame-masonry interface friction model, the linear stiffness modulus D_{11} was set with a value of 240 N/mm^3, while the linear stiffness modulus D_{22} was adjusted with a value of 400 N/mm^3. A cohesion of 3 MPa and a friction angle of 27° were calibrated for the interface with reference to some works in the literature, e.g. Okail et al. (2016) [18] and Sánchez-Tizapa (2009) [30]. Dilatancy and gap formation in the interface were not considered in order to reduce the number of variables and facilitate computational convergence. The models were considered to be calibrated once a reasonably good match between the numerical and experimental responses was obtained, see Fig. 6, as well as a simulated damage pattern of the walls consistent with the experimental one, see Fig. 7. The mechanical parameters of the different materials, after calibration of the models, are reported in Table 2.

The numerical against the experimental responses of the models of Walls 1–2 (4ϕ10 in tie-columns and vertical load of 100 kN) and Walls 3–4 (4ϕ16 and 200 kN) are compared in Figure 6. The numerical responses present a post-peak branch markedly different from that of the experimental responses, particularly for Walls 1–2, and even the experimental post-peak behaviour is different for similar walls, because of different crack paths in the walls. The numerical damage pattern is exemplified in Figure 7, with diagonal cracking developing through the masonry panel (Fig. 7a) and then the crack penetrating the beam-column joints (Fig. 7b), as is typical in CM walls and was observed in the tests by Zabala et al. (2004) [7], see Fig. 3. In the numerical model, diagonal tensile cracks are also observed at the wall corners opposite to the main diagonal cracking. The differences between the experimental and numerical force–displacement responses may be related with the uncertainty of the material properties, the heterogeneous nature of masonry and potential for local cracking, e.g. due to defects in the masonry fabric, and the limitations of the numerical model in dealing with this kind of phenomena.

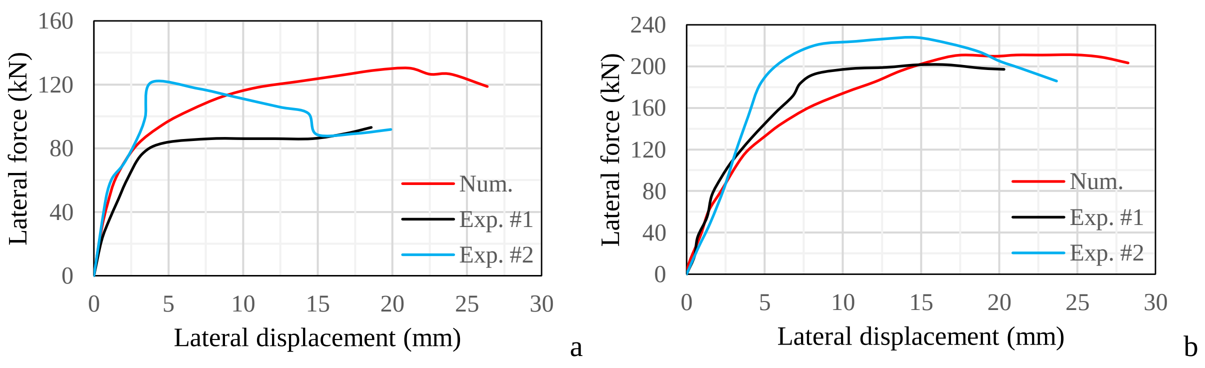

Figure 6. Numerical against experimental force–displacement responses for models of: (a) Walls 1–2 (4ϕ10 in tie-columns and vertical load of 100 kN) and (b) Walls 3–4 (4ϕ16 and 200 kN)

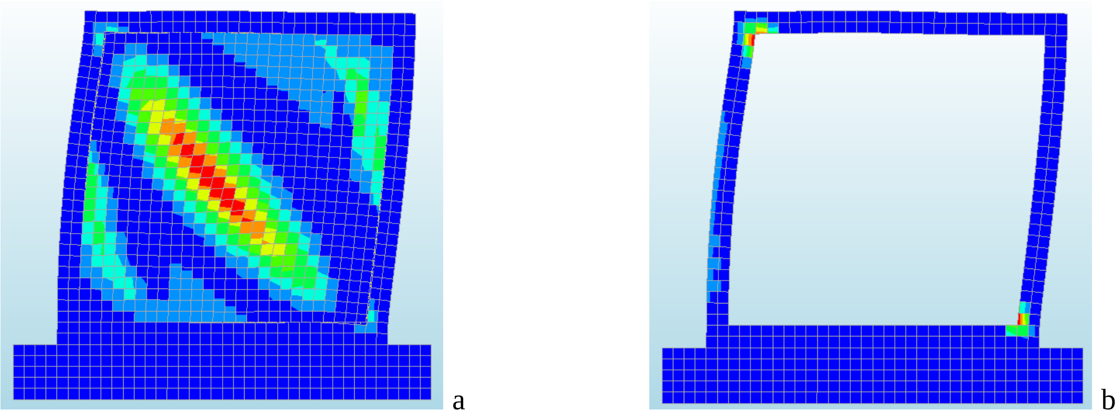

Figure 7. Contour plots of principal strains indicating the damage pattern at maximum lateral force for model of Walls 3–4 (4ϕ16 and 200 kN): (a) whole CM wall and (b) RC frame

Table 2. Mechanical parameters of materials for the CM wall models

	Concrete	Masonry	Steel	Interface
Elastic modulus, E (MPa)	30000	2000	200000	-
Compressive strength, f_m (MPa)	20	2.5	-	-
Compressive fracture energy, G_c (N/mm)	32	4	-	-
Tensile strength, f_t (MPa)	1.8	0.025	-	-
Tensile fracture energy, G_f^I (N/mm)	0.5	0.025	-	-
Linear stiffness modulus D_{11} (N/mm^3)	-	-	-	240
Linear stiffness modulus D_{22} (N/mm^3)	-	-	-	400
Cohesion (MPa)	-	-	-	3
Friction angle (º)	-	-	-	27

It needs to be noted that although many experimental tests are available in the literature, there is no known work which includes a comprehensive reporting of all values of material parameters used in the numerical model adopted in this study. The same model was used by Sánchez-Tizapa (2009) [30], but considering different values of the material parameters according to the experimental program carried out in that study, so it also works to demonstrate the reliability of the adopted numerical model. Therefore, further research is needed, including experimental testing for a detailed characterization of the values to adopt for specific material parameters, to allow for a more comprehensive validation of the used numerical model.

4. Parametric numerical study

After calibration of the numerical models, a parametric analysis was performed to study the influence of different variables on the composite behaviour of CM walls. Indeed, performance-based seismic design requires the consideration of different engineering demand parameters (EDPs), namely in terms of lateral force resistance, strain (as damage indicator) and stress patterns, and displacement capacity. By varying several influential parameters of the walls, as reported below, the values of EDPs are assessed in next subsections for different wall configurations.

4.1 Range of parameters

The behaviour of CM walls subjected to lateral in-plane loads is influenced by several variables, particularly the wall aspect ratio, the vertical load on the wall, the tie-column section and the longitudinal steel reinforcement in tie-columns. Here, the range of values for each of the considered parameters is defined. For the wall aspect ratio (H/L, where H and L are the wall height and length including the columns and beam depth, respectively), values of 1 and 1.5 were considered to be representative of current construction practice, and a value of 3 was considered to investigate the flexural behaviour of the walls. Values lower than 1 are possible, but in this case the failure is by diagonal shear, so a Coulomb-based formula may provide a suitable estimation of the shear resistance and can be extended to take into account the wall aspect ratio; see Marques and Lourenço (2019) [4].

Concerning the vertical stress on the wall (σ), values of 0.167 MPa and 0.667 MPa were assumed to be representative of low-rise buildings with lightweight slabs and mid-rise buildings with heavy slabs, respectively. For the tie-column section (*Tie-A*), the minimum cross-section in Eurocode 6 - Part 1-1 [31] was considered as lower bound, i.e. 150 mm along the face of the wall and 135 mm within the thickness of the wall (0.02 m^2); further, an intermediate section was considered with 150 x 200 mm^2 (0.03 m^2), and a upper bound of 200 x 200 m^2 (0.04 m^2) was considered to be representative of a higher flexural stiffness of the frame. Concerning the longitudinal steel reinforcement in tie-columns (A_s; a normalized reinforcement rate $\%A_s$ is also defined as A_s/A_c, where A_c is the tie-column cross-section), the minimum in Eurocode 6 - Part 1-1 was considered as lower bound, i.e. 4ϕ8 (201 mm^2), and a upper bound of 4ϕ12 (452 mm^2) was assumed (steel yield strength is 420 MPa). A total of 36 wall configurations were considered, according to the schematization presented in Figure 8.

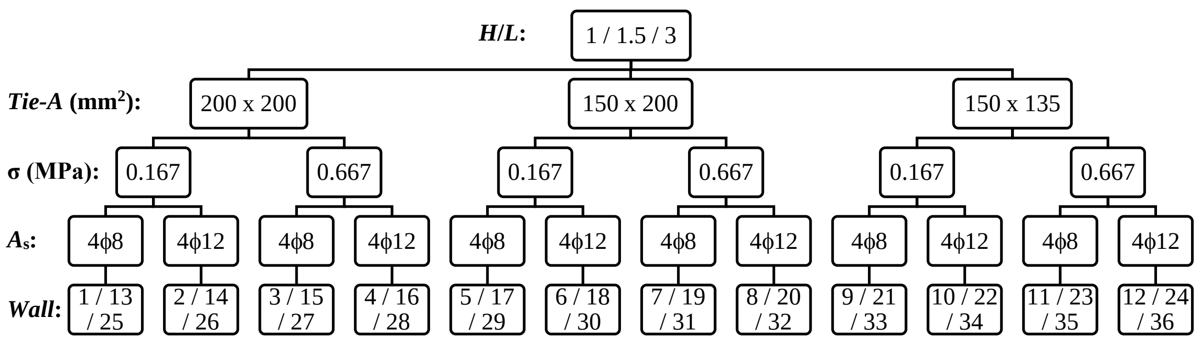

Figure 8. Schematization of the considered wall configurations

4.2 Pushover analysis and EDPs

The different wall configurations as described in the previous subsection were simulated under incremental lateral loading, i.e. using nonlinear static (pushover) analysis. The boundary and loading conditions of the walls were similar to the ones of the benchmark wall presented in Section 2.2, i.e. fixed at the base and free to rotate at the top, subjected to a constant vertical stress and with the horizontal load applied at the tie-beam level. The regular Newton-Raphson method with an error tolerance of 10^{-3} according to an energy convergence criterion was adopted for the solver in DIANA [22]. The results were processed in order to plot the lateral force (sum of lateral reactions at the wall base) against the lateral displacement of the wall at the tie-beam level, i.e. the lateral force–displacement response (pushover curve). The pushover curves for all CM wall configurations considered in the parametric study are presented in Figure 9.

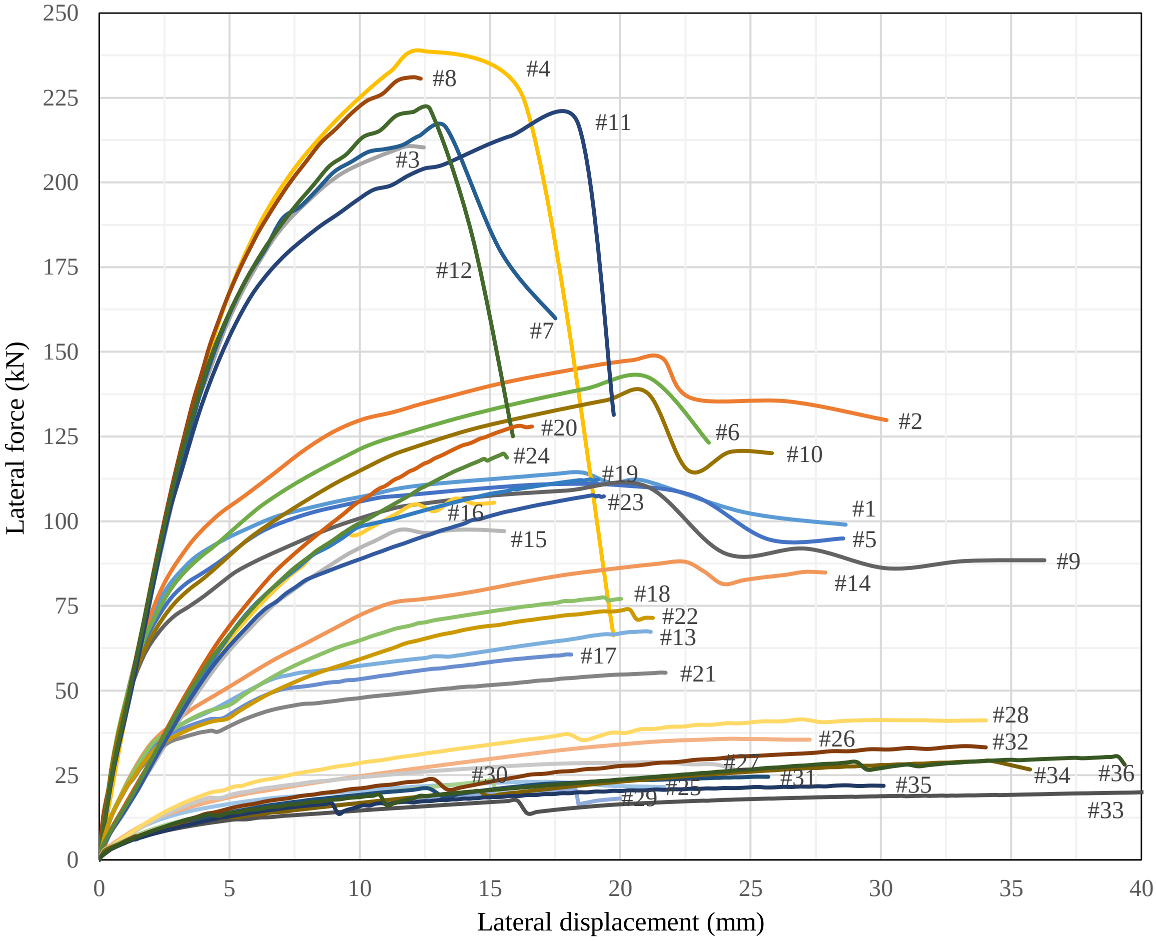

Figure 9. Pushover curves for all wall configurations

Although a wide range of wall responses is observed in Figure 9, in terms of initial stiffness, lateral resistance and displacement capacity, some trends can be identified. The ultimate displacement, although it may to some extent be influenced by computational convergence issues, decreases as the initial stiffness and the lateral resistance of the walls increase, which is mainly the case of square walls. Contrarily, for slender walls, although the values of lateral resistance are low, a large displacement capacity is observed.

The pushover curves denote that convergence was not reached for all walls up to a condition representative of the ultimate state of each wall (usually defined for a displacement corresponding to a decay of 20% in the maximum lateral force). Furthermore, considering the possible limitations of the used modelling approach in accurately simulating the wall response in displacement, hereafter, for comparison purposes and derivation of predictive models only the response branch up to the peak point is considered. The lateral force at this point (i.e. the lateral resistance), F_{max}, and the corresponding displacement, d_{max}, are reported in Table 3 for all walls.

Table 3. Characteristics of the wall configurations and values of the peak point on the pushover curves

#	L (m)	H/L	*Tie-A* (mm^2)	l (m)	σ (MPa)	A_s	%A_s	F_{max} (kN)	d_{max} (mm)
1	3	1	200 x 200	2.6	0.167	4ϕ8	0.50	114.34	18.6
2						4ϕ12	1.13	148.17	21.6
3					0.667	4ϕ8	0.50	210.70	11.8
4						4ϕ12	1.13	238.82	12.4
5			150 x 200	2.7	0.167	4ϕ8	0.67	110.90	17.2
6						4ϕ12	1.51	142.46	21.1
7					0.667	4ϕ8	0.67	216.26	13.3
8						4ϕ12	1.51	231.06	12.0
9			150 x 135	2.7	0.167	4ϕ8	0.99	110.31	21.0
10						4ϕ12	2.23	137.73	21.1
11					0.667	4ϕ8	0.99	217.39	18.4
12						4ϕ12	2.23	221.65	12.7
13	2	1.5	200 x 200	1.6	0.167	4ϕ8	0.50	67.50	21.0
14						4ϕ12	1.13	88.07	22.5
15					0.667	4ϕ8	0.50	97.48	11.6
16						4ϕ12	1.13	106.65	13.7
17			150 x 200	1.7	0.167	4ϕ8	0.67	60.67	17.9
18						4ϕ12	1.51	77.49	19.4
19					0.667	4ϕ8	0.67	112.31	18.9
20						4ϕ12	1.51	128.16	16.2
21			150 x 135	1.7	0.167	4ϕ8	0.99	55.31	21.5
22						4ϕ12	2.23	73.90	20.4
23					0.667	4ϕ8	0.99	107.65	19.0
24						4ϕ12	2.23	119.92	15.5
25	1	3	200 x 200	0.6	0.167	4ϕ8	0.50	23.06	16.3
26						4ϕ12	1.13	35.77	24.3
27					0.667	4ϕ8	0.50	28.85	21.3
28						4ϕ12	1.13	41.47	27.0
29			150 x 200	0.7	0.167	4ϕ8	0.67	20.76	18.3
30						4ϕ12	1.51	23.39	15.1
31					0.667	4ϕ8	0.67	24.56	25.2
32						4ϕ12	1.51	33.59	33.3
33			150 x 135	0.7	0.167	4ϕ8	0.99	20.20	42.1
34						4ϕ12	2.23	29.26	34.2
35					0.667	4ϕ8	0.99	22.01	28.7
36						4ϕ12	2.23	30.50	39.1

How to cite: Marques, R., Pereira, J. M., Lourenço, P. B. (2020). Lateral in-plane seismic response of confined masonry walls: From numerical to backbone models. Engineering Structures, 221, 111098. doi:10.1016/j.engstruct.2020.111098

4.2.1 Lateral resistance

A comprehensive comparison of results is difficult to do only with reference to Figure 9 and to the values listed in Table 3. So, since from Figure 9 it seems to exist a segmentation of the capacity curves in terms of the initial stiffness of the CM walls, a division is made in six groups of walls. The pushover curves for each group of walls are presented in Figure 10. The several groups are listed in Table 4, where, beyond the parameters of each wall, a comparison is made in terms of the maximum lateral force, F_{max}, and the improvement factor for each wall in terms of F_{max}, IF_{max}, within each group relatively to an adopted reference wall (R). The (R) sample is the one that, within each group, has the lowest rate of longitudinal steel in tie-columns, i.e. largest cross-sectional area of tie-column and lowest area of steel reinforcement. The groups are established mainly in terms of σ for walls with H/L up to 1.5, while for the more slender walls (H/L = 3) the groups are defined in terms of *Tie-A*.

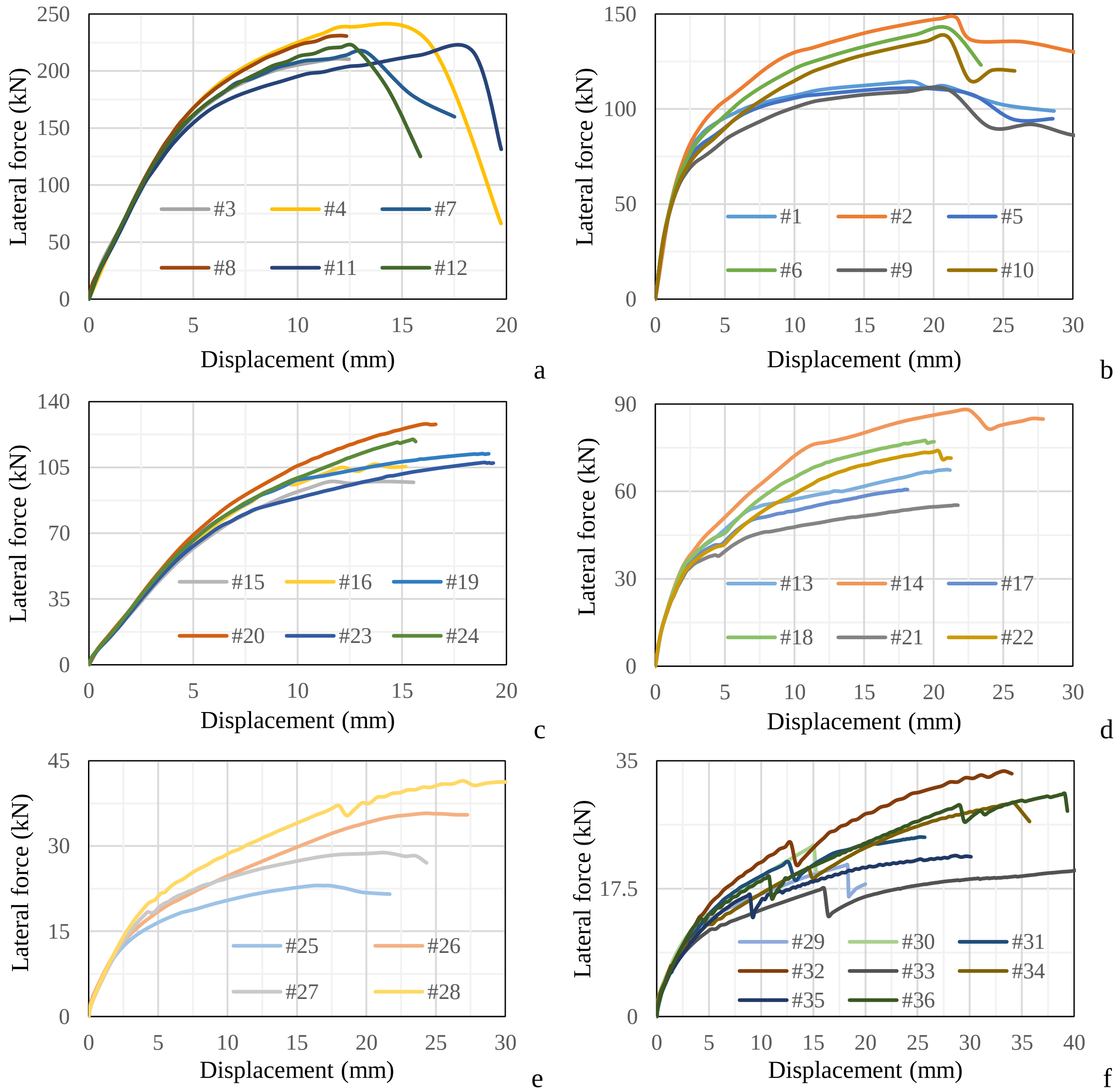

Figure 10. Pushover curves of walls with: (a) H/L = 1, σ = 0.667 MPa (Group 1); (b) H/L = 1, σ = 0.167 MPa (Group 2); (c) H/L = 1.5, σ = 0.667 MPa (Group 3); (d) H/L = 1.5, σ = 0.167 MPa (Group 4); (e) H/L = 3, *Tie-A* = 200 x 200 mm^2 (Group 5); (f) H/L = 3, *Tie-A* = 150 x 135 to 150 x 200 mm^2 (Group 6)

Table 4. Characteristics and lateral resistance of wall configurations within the identified groups

#	L (m)	H/L	*Tie-A* (mm^2)	l (m)	σ (MPa)	A_s	%A_s	F_{max} (kN)	IF_{max}
Group 1									
3(R)	3	1	200 x 200	2.6	0.667	$4\phi8$	0.50	210.70	1.000
4						$4\phi12$	1.13	238.82	1.133
7			150 x 200	2.7		$4\phi8$	0.67	216.26	1.026
8						$4\phi12$	1.51	231.06	1.097
11			150 x 135	2.7		$4\phi8$	0.99	217.39	1.032
12						$4\phi12$	2.23	221.65	1.052
Group 2									
1(R)	3	1	200 x 200	2.6	0.167	$4\phi8$	0.50	114.34	1.000
2						$4\phi12$	1.13	148.17	1.296
5			150 x 200	2.7		$4\phi8$	0.67	110.90	0.970
6						$4\phi12$	1.51	142.46	1.246
9			150 x 135	2.7		$4\phi8$	0.99	110.31	0.965
10						$4\phi12$	2.23	137.73	1.205
Group 3									
15(R)	2	1.5	200 x 200	1.6	0.667	$4\phi8$	0.50	97.48	1.000
16						$4\phi12$	1.13	106.65	1.094
19			150 x 200	1.7		$4\phi8$	0.67	112.31	1.152
20						$4\phi12$	1.51	128.16	1.315
23			150 x 135	1.7		$4\phi8$	0.99	107.65	1.104
24						$4\phi12$	2.23	119.92	1.230
Group 4									
13(R)	2	1.5	200 x 200	1.6	0.167	$4\phi8$	0.50	67.50	1.000
14						$4\phi12$	1.13	88.07	1.305
17			150 x 200	1.7		$4\phi8$	0.67	60.67	0.899
18						$4\phi12$	1.51	77.49	1.148
21			150 x 135	1.7		$4\phi8$	0.99	55.31	0.819
22						$4\phi12$	2.23	73.90	1.095
Group 5									
25(R)	1	3	200 x 200	0.6	0.167	$4\phi8$	0.50	23.06	1.000
26						$4\phi12$	1.13	35.77	1.551
27					0.667	$4\phi8$	0.50	28.85	1.251
28						$4\phi12$	1.13	41.47	1.799
Group 6									
29(R)	1	3	150 x 200	0.7	0.167	$4\phi8$	0.67	20.76	1.000
30						$4\phi12$	1.51	23.39	1.127
31					0.667	$4\phi8$	0.67	24.56	1.183
32						$4\phi12$	1.51	33.59	1.618
33			150 x 135	0.7	0.167	$4\phi8$	0.99	20.20	0.973
34						$4\phi12$	2.23	29.26	1.409
35					0.667	$4\phi8$	0.99	22.01	1.061
36						$4\phi12$	2.23	30.50	1.469

The walls in Group 1 have the largest values of F_{max} (210 to 239 kN) although the drop of lateral force occurs for a reduced displacement (15–20 mm). Contrarily, the walls in Group 6 present the lowest values of F_{max} (20–34 kN); furthermore, at about half of the resistance (for around 15–20 mm) there is a small force drop (15–18 %), after that the lateral force increases up to F_{max} (with d_{max} around 25–40 mm). For the remaining groups, the values of F_{max} and ultimate displacement are in between the intervals observed for Groups 1 and 6, and their capacity curves present a growing branch up to F_{max}, with the exception of Group 2 which presents a small force drop after F_{max} is reached (10–20 %).

From Table 4, it is observed that in Group 1 (with σ = 0.667 MPa) there is no apparent advantage in have larger *Tie-A*, since IF_{max} is always larger than 1 and even may increase if *Tie-A* is lower, although the increase of %A_s is more effective in increasing IF_{max} if *Tie-A* is larger. The contrary occurs for Group 2 (with σ = 0.167 MPa), since IF_{max} decreases if *Tie-A* is lower, while the increase of %A_s is also in this case more effective if *Tie-A* is larger. In Group 3 (with σ = 0.667 MPa) there is no apparent advantage in have *Tie-A* larger than 150 x 200 mm^2, and the increase of %A_s is more effective in increasing IF_{max} if *Tie-A* is lower. In Group 4 (with σ = 0.167 MPa), the lower σ makes IF_{max} to be lower than 1 for walls with smaller values of *Tie-A* and %A_s. For Groups 5 and 6 (with both σ values) it is observed that, in general, the increase of *Tie-A* and particularly %A_s allows to increase IF_{max}, and also to some extent the displacement capacity. Summarily, for square walls subjected to high σ there is no advantage in increasing *Tie-A*, unless A_s is increased; for square walls subjected to low σ the increase of *Tie-A* allows increasing of F_{max}; for walls with H/L = 3 the increase of *Tie-A* and A_s allows an even better enhancement of F_{max}; and for walls with H/L = 1.5, an intermediate situation is observed depending on the σ value.

Aiming at a better comparison of the response of the walls up to the peak point, the pushover curves up to F_{max} (normalized to 1) are presented in Figure 11; the relative displacement over the wall height (drift) is given in the horizontal scale. Among the different walls, F_{max} is reached for a very wide interval of lateral displacement (0.4–1.4 % drift), meaning that the walls develop their resistance for different displacement levels. Walls with larger initial stiffness reach in general F_{max} for a smaller drift. Furthermore, scatter plots of F_{max} versus H/L and F_{max} versus *Tie-A* are presented in Figure 12. H/L has a large influence on F_{max} and, for any H/L ratio, the lowest force values occur for σ-A_s combination '0.167 MPa-4ϕ8' while the largest ones occur for '0.667 MPa-4ϕ12' (Fig. 12a). *Tie-A* has a less evident influence on F_{max} because of the associated effect of σ and A_s, but a general trend of increasing F_{max} with *Tie-A* is observed in Figure 12b, with the exception of the values for combination '0.667 MPa-4ϕ8'.

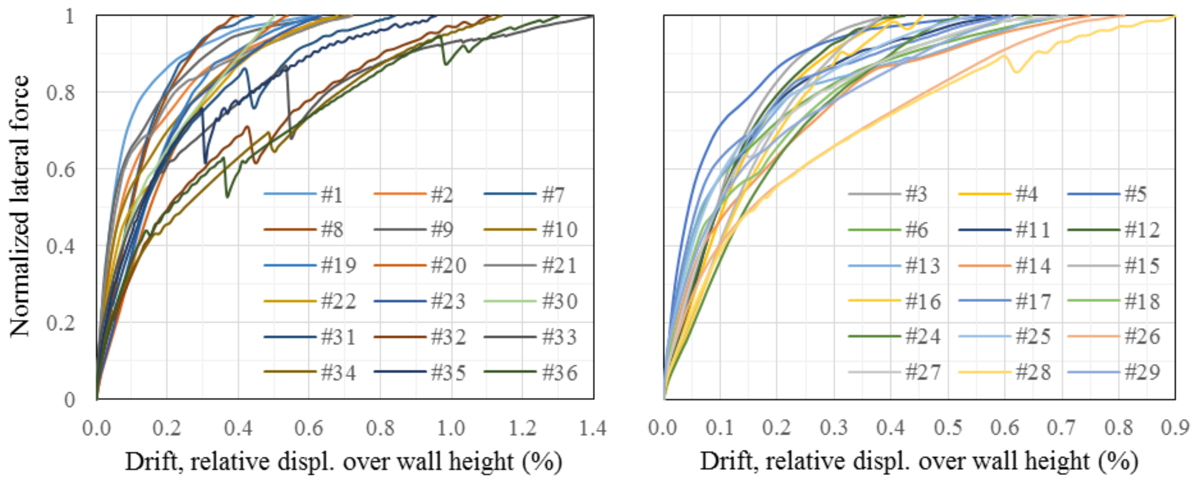

Figure 11. Pushover curves of the walls up to the normalized maximum lateral force

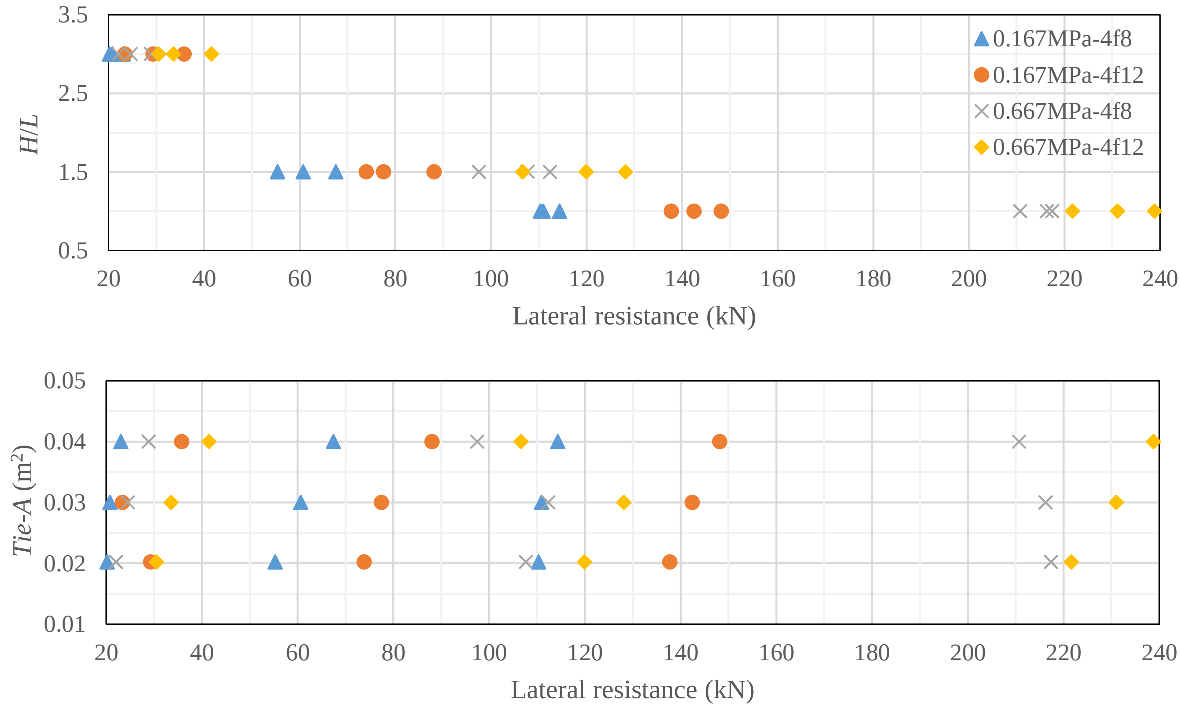

a

b

Figure 12. Scatter plots of lateral resistance vs. (a) *H*/*L* ratio and (b) *Tie-A* area

4.2.2 Strain and stress patterns

A damage pattern by diagonal cracking is apparently observed for all CM walls, based on the contour plots of principal strains presented in Figure 13. However, as *H*/*L* increases the cracking is more diffused through the height of the wall because of the formation of vertical cracks due to bending. This failure mechanism with combined diagonal and vertical cracks is also evidenced from the experimental work by Varela-Rivera et al. (2019) [3] and from the numerical work by Tripathy and Singhal (2019) [6]. In the performed numerical simulations, yielding of longitudinal steel reinforcement in tie-columns was in general not reached, contrarily to what was experimentally observed by Varela-Rivera et al. (2019) [3]. Tripathy and Singhal (2019) [6], based on their numerical work, conclude that for CM walls with a higher amount of reinforcement, yielding of steel may not occur even after the wall failure.

Indeed, the efficiency of the steel reinforcement may depend on the particular characteristics of the CM wall. In the performed simulations, for the longitudinal reinforcement in tie-columns, the reached stress (σ_s) to yielding stress (f_y) ratio, $R = \sigma_s/f_y$, decreases as *H*/*L* increases, and particularly if A_s is higher; e.g. for Wall #9 (H/L = 1, A_s = 4ϕ8): R = 1.0, Wall #10 (H/L = 1, A_s = 4ϕ12): R = 0.8, Wall #21 (H/L = 1.5, A_s = 4ϕ8): R = 0.62, Wall #22 (H/L = 1.5, A_s = 4ϕ12): R = 0.44, Wall #33 (H/L = 3, A_s = 4ϕ8): R = 0.48, Wall #34 (H/L = 3, A_s = 4ϕ12): R = 0.32. The R ratio can be understood as an efficiency factor of the longitudinal reinforcement in tie-columns. It is further addressed later in this work, in a proposal for the flexural resistance of CM walls.

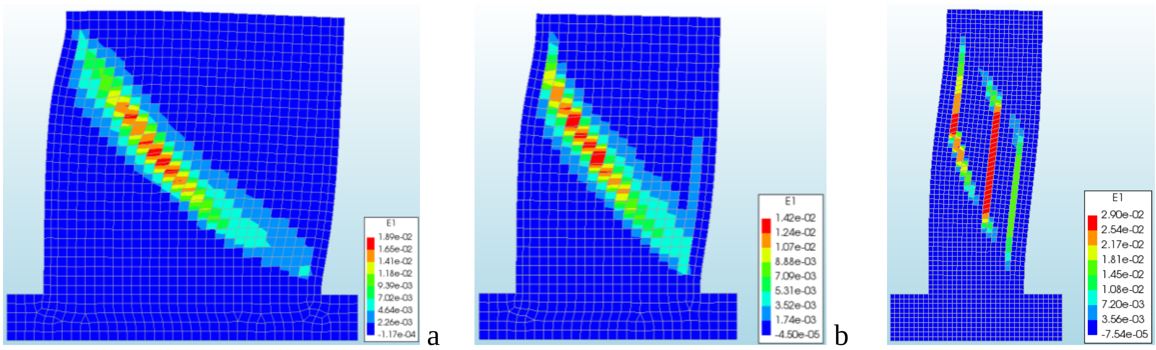

Figure 13. Numerical crack pattern at F_{max} of CM walls with *H*/*L*: (a) 1, (b) 1.5 and (c) 3; σ = 0.167 MPa

A CM wall presents a combined shear-flexural mechanism in which the extent of each behavioural component (shear and flexure) depends on the wall characteristics, like *H*/*L*, σ, *Tie-A*, A_s and also the frame-masonry connection. Under the combined mechanism, even if the masonry panel is damaged there is a fraction of the panel that remains elastic and reacts against the wall base, similarly to what is proposed by Tomaževič and Klemenc (1997) [32]; see vertical stress plots in Fig. 14 and stress diagrams in Fig. 15. The plots in Figure 14 allow to observe the path and distribution of vertical stresses on the masonry panels of walls with different *H*/*L* values. For all walls, vertical compressive stresses tend to distribute within strips adjacent to the loaded diagonal of the masonry panel. In the walls with *H*/*L* up to 1.5, concentration of high stresses is observed in the compressed lower corner of the masonry panel. For the more slender wall, compressive stress sub-vertical strips also develop around the panel diagonal. Moreover, the vertical compressive stresses are well distributed at the masonry panel top, while the masonry panel is only partially compressed at the base.

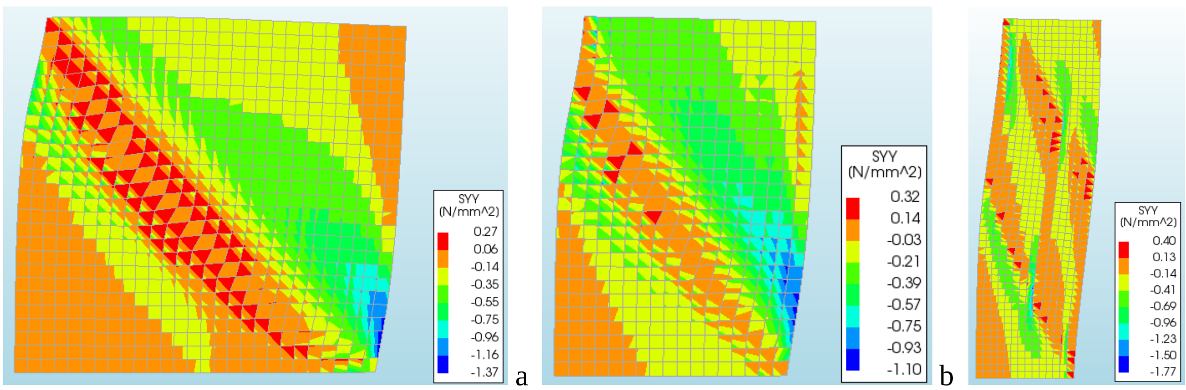

Figure 14. Vertical stresses on the masonry panel at F_{max} for walls with *H*/*L*: (a) 1, (b) 1.5 and (c) 3; σ = 0.167 MPa

The vertical stress profiles at the base of the masonry panel of the different walls are presented in Figure 15. It is observed that the compressed length of the panel base depends on the *H*/*L* and σ values; while the compressed length increases with increasing *H*/*L*, it seems to reduce with increasing σ. The graphs in Figure 15 denote that the distribution of stresses at the wall base can be approached as a triangular diagram of stresses, similarly to what is proposed by Tomaževič and Klemenc (1997) [32], see Fig. 16a. However, it is observed in Figure 15 that the compressive stress at the right edge of the masonry panel is restrained by the tie-element connection, comparatively to the maximum compressive stress which occurs at a section that is slightly inside the cross-section of the masonry panel, at the right end. In any case, based on the extracted results, the relative compressed length of the masonry panel, l_c, can be related with H/L as presented in Figure 16b, where formulas to calculate l_c are also provided as the best fit according to a linear regression by least squares. For a given σ, l_c increases with H/L, while for an σ of 0.667 MPa a linear relation between l_c and H/L is observed.

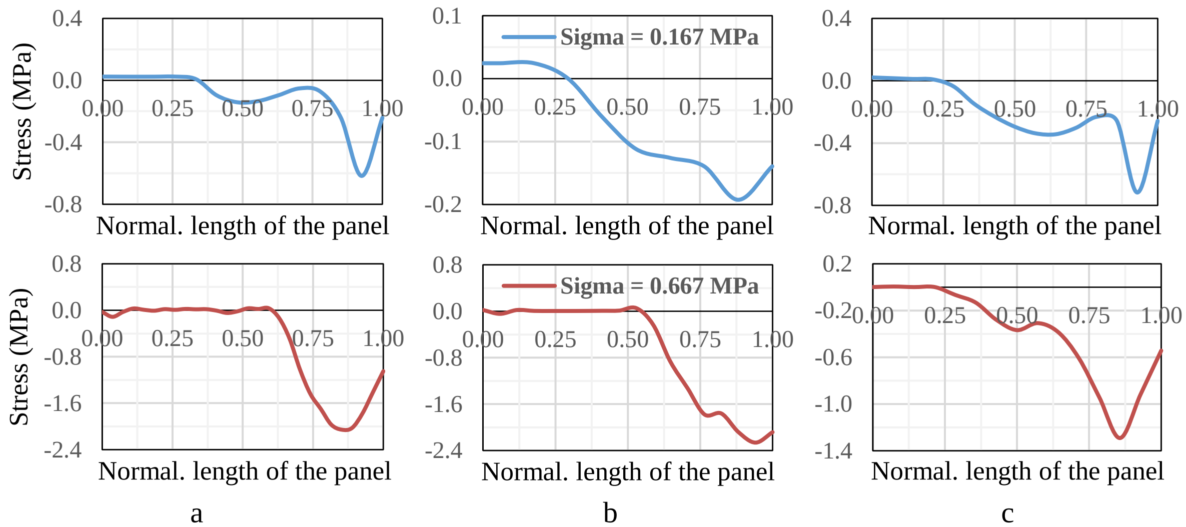

Figure 15. Stresses at the base of the masonry panel at F_{max} for walls with H/L: (a) 1, (b) 1.5 and (c) 3

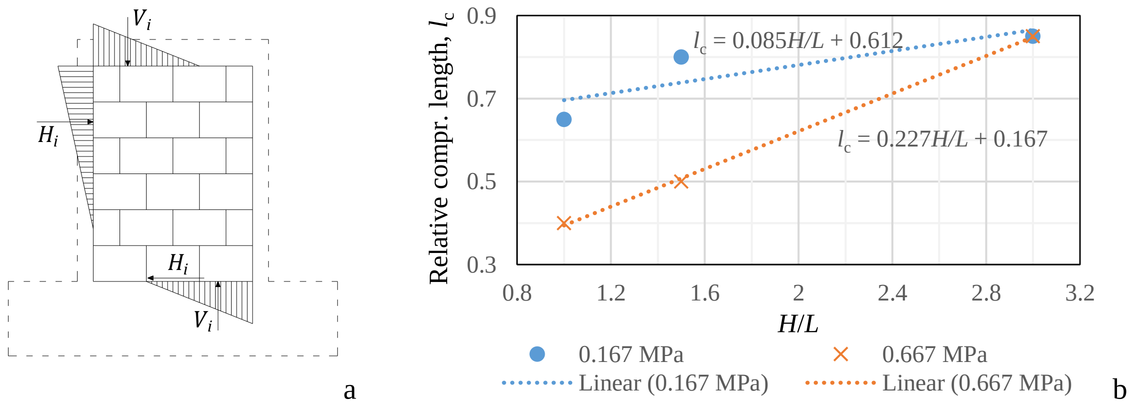

Figure 16. Compressive stress diagrams for CM wall: (a) interaction stresses around masonry panel (from Tomaževič and Klemenc (1997) [32]) and (b) relationships between l_c and H/L

4.2.3 Displacement capacity

In modern design codes the displacement capacity is adopted as the basis of performance-based seismic assessment, since the response in displacement allows to directly assess the inelastic capacity of a given structure, e.g. through a ductility measure, which is not possible with considering only the lateral resistance; see Priestley et al. (2007) [33]. Such an approach is mainly applicable to structures with integral behaviour, i.e. all structural elements contribute to the lateral resistance up to a controlled damage level and allowing load redistribution between them. In the case of CM walls, the masonry panel presents a composite behaviour with the tie-elements up to a significant displacement level, even after the decay of the frame-masonry connection.

Here, because of the complexity and uncertainty in defining the displacement at which that decay occurs with an important loss of lateral resistance, the displacement at the peak force, d_{max}, is taken as a representative measure to consider in a backbone model of the lateral force–displacement response. The post-peak branch can then be defined with basis on rules derived from experimental results in the literature. The sensitivity of d_{max} to the *H*/*L* and *Tie*-*A* values is denoted in the scatter plots in Figure 17. It seems to exist an increasing trend for d_{max} as *H*/*L* increases, mainly if $\sigma = 0.667$ MPa and A_s is 4ϕ12, and it also looks that d_{max} decreases as *Tie*-*A* increases, mainly if $\sigma = 0.667$ MPa and A_s is 4ϕ8. Although the similar plots in terms of ultimate displacement are not presented here, since it was not possible to obtain it for given walls due to convergence loss, the trends were similar but with much more scatter. The relationship between d_{max} and the ultimate displacement will be addressed in the next section.

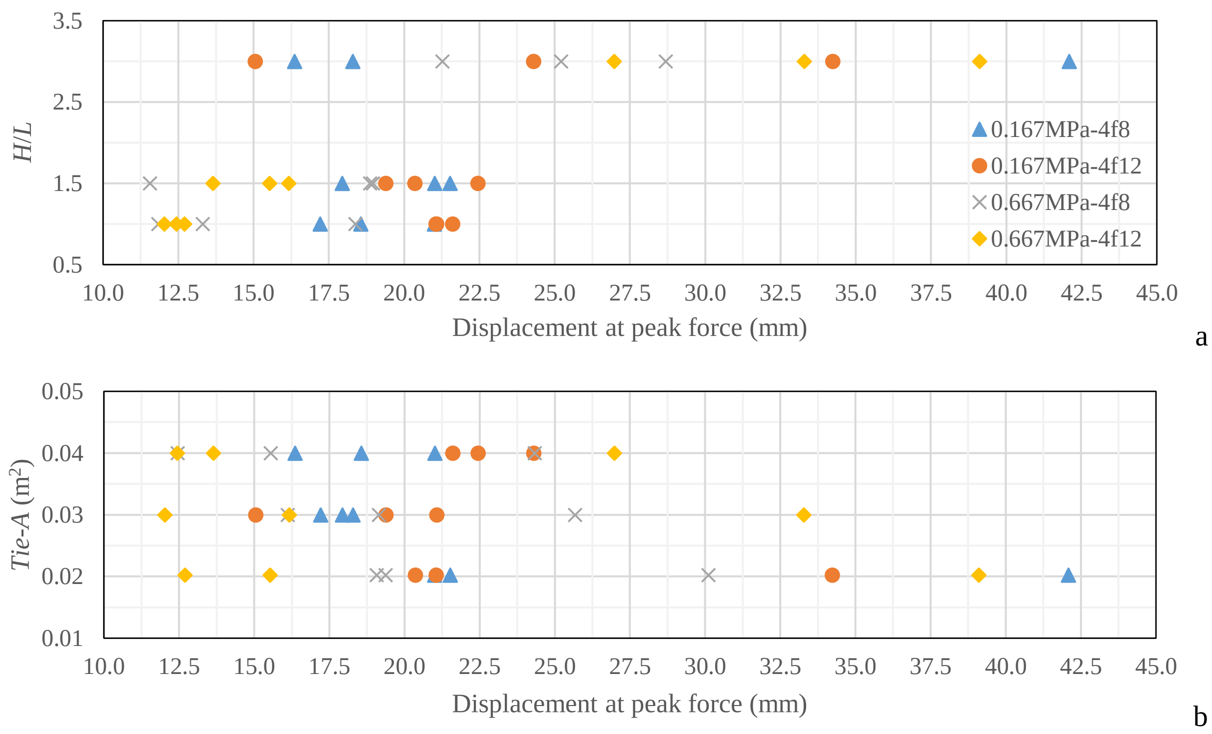

Figure 17. Scatter plots of displacement at peak force vs. (a) *H*/*L* ratio and (b) *Tie*-*A* area

5. Predictive analytical models

This section is intended to propose suitable analytical models to predict the lateral force–displacement response of CM walls. The formulas proposed in the literature for estimation of the force resistance and displacement capacity of CM walls subjected to lateral in-plane loading are mostly applicable to squat walls, whose response is governed by a shear failure mechanism. A review of such formulas can be found in Marques and Lourenço (2013) [34] and Riahi et al. (2009) [35]. However, a flexural failure or even a mixed shear-flexural failure are also possible mechanisms, so suitable analytical models to describe them are needed. In the following, new proposals for estimation of both the force resistance and displacement capacity of CM walls subjected to lateral in-plane loading, as well as a discussion and proposal of suitable lateral force–displacement backbone models, are presented.

5.1 Lateral resistance

The lateral resistance of a CM wall is here defined as the maximum lateral force that it can withstand. This load depends on the type of failure mechanism of the wall, which typically can be through diagonal shear, flexural failure, sliding shear or a combination of them. The activation of a given mechanism depends on the characteristics of both the masonry panel and tie-elements, as well as of its connection. In the case of squat walls, the diagonal shear mechanism may be determinant and the shear resistance can be calculated using a Coulomb-based formula for ease of use, like in Equation (1).

$$V_s = (f_{vk0} + 0.4\, \sigma_d)\, A_w \tag{1}$$

where

f_{vk0} is the characteristic initial shear strength of masonry, under zero compressive stress;

σ_d is the design compressive stress on the wall, at the level under consideration;

A_w is the gross cross-sectional area of the wall, including the tie-columns.

For slender walls ($H/L \geq 1.5$), a flexural or even combined shear-flexural mechanism is expected to occur. The theoretical flexural resistance of reinforced masonry (RM) walls is given by Equation (2), based on the equilibrium of forces on the wall section (considering steel yielding). However, according to the simulations performed here and experimental evidence reported before, yielding of longitudinal reinforcement in tie-columns is in general not reached, so the lateral resistance is overestimated when using Equation (2). For a better estimate, a formulation can be derived by assuming the entire wall section made of a same material, and a rectangular compressive stress block based on the design strength of masonry or concrete, whichever is the lesser, as given by Equations (3–4); see Fig. 18. A factor may be further included in the formulation to take into account the efficiency of the reinforcement in tie-columns, as given in Equations (5–6), i.e. the yield force of reinforcement is multiplied by the square root of $(H/L)^{-1}$. A comparison of estimates of the lateral resistance of CM walls from different analytical approaches against the predicted resistances from the numerical simulations is made in Figure 19.

$$M_{\mathrm{Rd,RM}} = A_s\, f_{yd}\, z + \frac{\sigma_d t L^2}{2}\left(1 - \frac{\sigma_d}{f_d}\right) = A_s\, f_{yd}\, z + N_{\mathrm{Ed}}\left(\frac{L}{2} - 0.5\frac{\sigma_d L}{f_d}\right) \tag{2}$$

where

A_s is the area of vertical reinforcement, symmetrically placed at both ends;

f_{yd} is the design yield strength of reinforcement;

z is the distance between the centroids of reinforcement at the ends;

N_{Ed} is the design value of the vertical load;

t is the thickness of the wall;

L is the length of the wall;

f_d is the design compressive strength of masonry or concrete, whichever is the lesser.

$$M_{Rd,CM} = A_s\, f_{yd}\, (d - 0.4x) + N_{Ed}\, \left(\frac{L}{2} - 0.4x\right) \quad (3)$$

$$N_{Ed} = F_c - F_s \quad \Leftrightarrow \quad x = \frac{N_{Ed} + A_s\, f_{yd}}{0.8 \eta_f f_d\, t} \quad (4)$$

where

d is the effective depth of the wall cross-section;

x is the depth to the neutral axis of the wall section;

F_c is the resultant of compressive stresses in the wall section;

F_s is the tensile force of tensioned reinforcement at yielding;

η_f is the factor defining the equivalent rectangular stress block, assumed equal to 0.85.

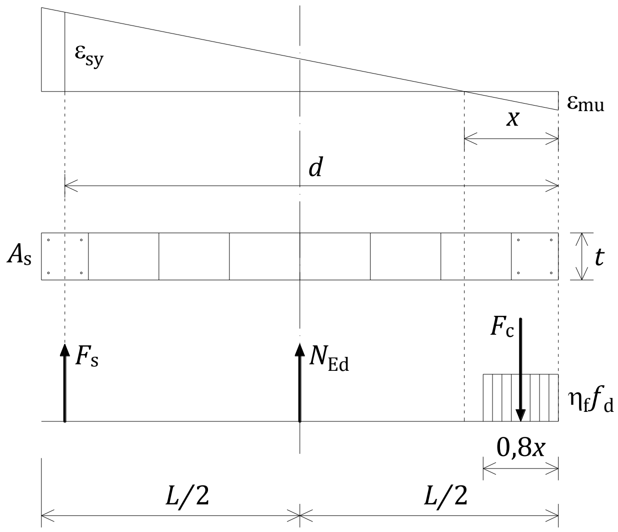

Figure 18. Stress and strain distributions assumed on the section of a CM wall in bending

$$M_{Rd,CM} = A_s\, f_{yd}\, \sqrt{L/H}\, (d - 0.4x\,) + N_{Ed}\, \left(\frac{L}{2} - 0.4x\right) \quad (5)$$

$$N_{Ed} = F_c - F_s \quad \Leftrightarrow \quad x = \frac{N_{Ed} + A_s\, f_{yd}\, \sqrt{L/H}}{0.8 \eta_f f_d\, t} \quad (6)$$

where H is the height of the wall.

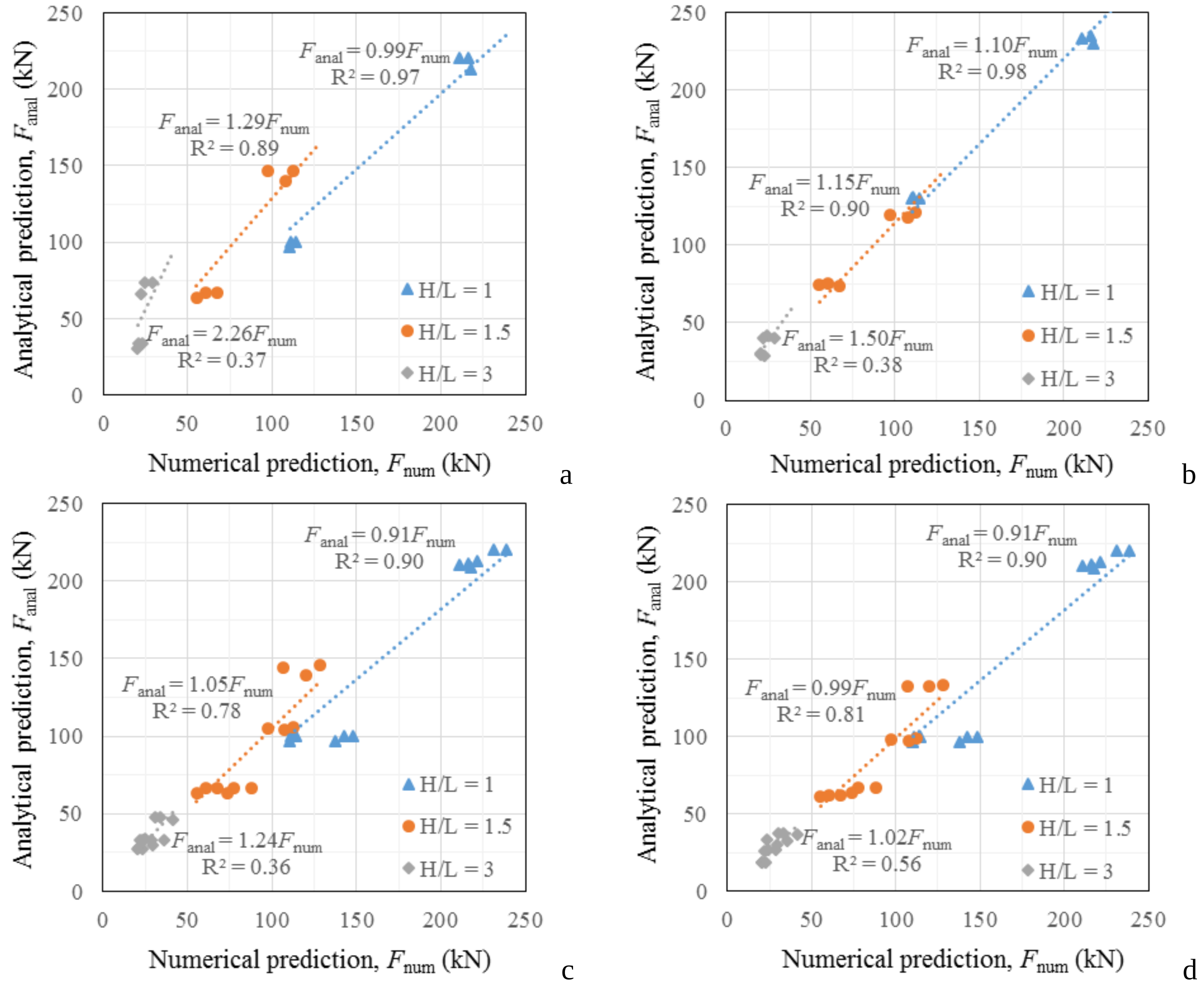

Figure 19. Analytical vs. numerical predictions of the lateral resistance according to (a) shear Eq. (1) and (b) flexural Eq. (2) (only for walls with A_s = 4ϕ8), and (c) min. (shear Eq. (1), flexural Eq. (3)) and (d) min. (shear Eq. (1), modified flexural Eq. (5)) for all walls

It is observed in Figure 19a that when using the typical formula to calculate the shear resistance of URM walls (Eq. (1)), the deviation from the numerical predictions increases as H/L is larger. If the flexural formula for RM walls (Eq. (2)) is used, a similar trend is verified in Figure 19b, but with much lower deviation from the numerical predictions, meaning that the flexural strength mechanism may be determinant for the response of slender walls. Indeed, the lateral resistance should be obtained from calculating both the shear and flexural strength domains, and the lower of them determines the failure mechanism of the wall and the associated resistance.

This last procedure allows a better match between analytical and numerical predictions (Fig. 19c); Equation (3) is used in this case instead of Equation (2) because it provides an overall better estimate of the flexural resistance. However, the best match is obtained when, beyond the consideration of both the shear and flexural strength domains, the formula proposed in Equation (5) for the flexural resistance is used (Fig. 19d). In this case, for any of the H/L values a relatively good approximation of the analytical results to the numerical ones is obtained, although the coefficient of determination (R^2) for the set of more slender walls is below 0.6. For these walls, a mixed shear-flexural failure mechanism may occur, most likely requiring a new formulation to consider it, to be addressed in future studies.

5.2 Displacement capacity

With the raising awareness of sustainable design, displacement-based methods are increasingly used for structural design of buildings, allowing to exploit most of the materials strength and inelastic capacity of structural members. Although many research works, both experimental and theoretical, have been carried out on the in-plane response of masonry walls, these studies have mainly focused on the force characteristics of the walls. Only recently are the displacement characteristics of the in-plane response of masonry walls attracting the attention of researchers. Indeed, the deformation capacity is a key parameter in seismic design and assessment of masonry structures. The current state of knowledge of the deformation capacity of structural masonry is limited, since it is a very complex parameter which is influenced not only by the failure mechanism, but by many other factors such as the constituent materials, geometry, pre-compression level, etc.

A few studies for formulation of the displacement capacity of URM walls have been developed, e.g. Petry and Beyer (2015) [36]. The displacement of CM walls is an even more complex topic, since it involves a multipart interaction between the masonry panel and the tie-elements through a common interface. Currently, it is hardly possible to take into account all factors influencing the deformation capacity of CM walls due to inhomogeneous experimental data and a lack of reliable mechanical models. Several authors, i.e. Yekrangnia et al. (2017) [37], Ranjbaran et al. (2012) [13] and Riahi et al. (2009) [35], have proposed different formulas to estimate the displacement capacity of CM walls, which are however difficult to generalize to all wall configurations. Indeed, the formulas proposed by Yekrangnia et al. (2017) [37] and Riahi et al. (2009) [35] are only applicable to shear-dominated walls and the ones proposed by Ranjbaran et al. (2012) [13] have been adjusted with a limited amount of data.

In the following, based on the numerical results for the considered range of wall configurations, in particular by varying H/L, charts for estimation of the drift at the peak force of CM walls, δ_{max}, are proposed, similarly to the idea by Turgay et al. (2014) [38] for RC frames with masonry infill walls. After filtering the plots of the relation between δ_{max} and H/L for identified walls, two independent charts are proposed for CM walls subjected to normalized vertical stress (σ/f_m) values of 0.267 and 0.067, respectively in Figures 20 and 21, with a separation also made in terms of reinforcement rate ranges (i.e. $\%A_s$ intervals of 0.5–1.0 % and 1.1–2.2 %). The proposed limits of δ_{max} as a function of H/L are the lower bound of the relations for the corresponding wall configurations. Thus, after δ_{max} is defined, the ultimate drift, δ_{ult}, can be estimated by assuming a value for the $\delta_{ult}/\delta_{max}$ ratio, as it will be discussed later.

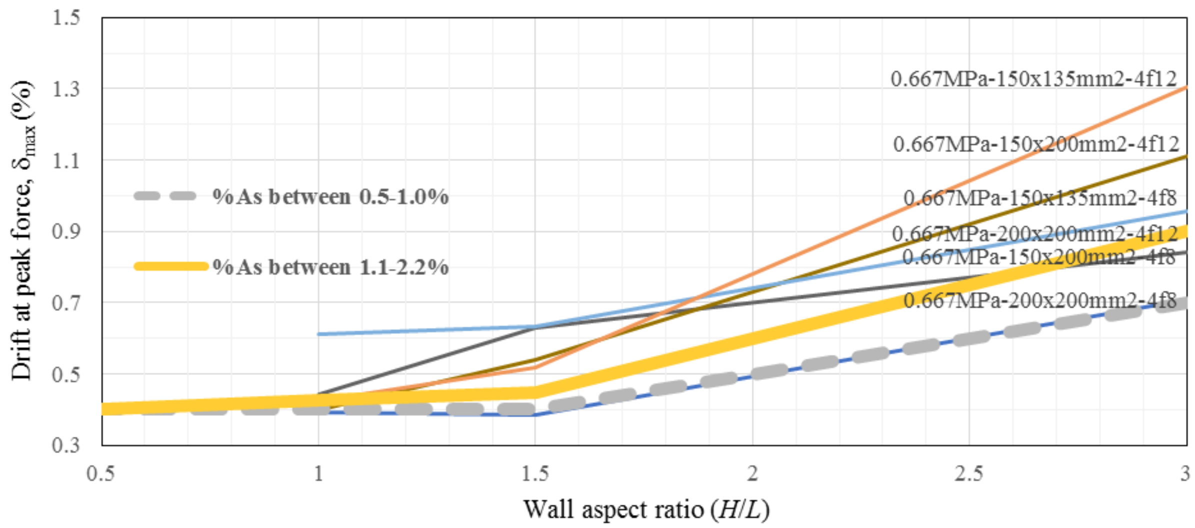

Figure 20. Charts for estimation of δ_{max} for CM walls with a normalized vertical stress $\sigma/f_m = 0.267$

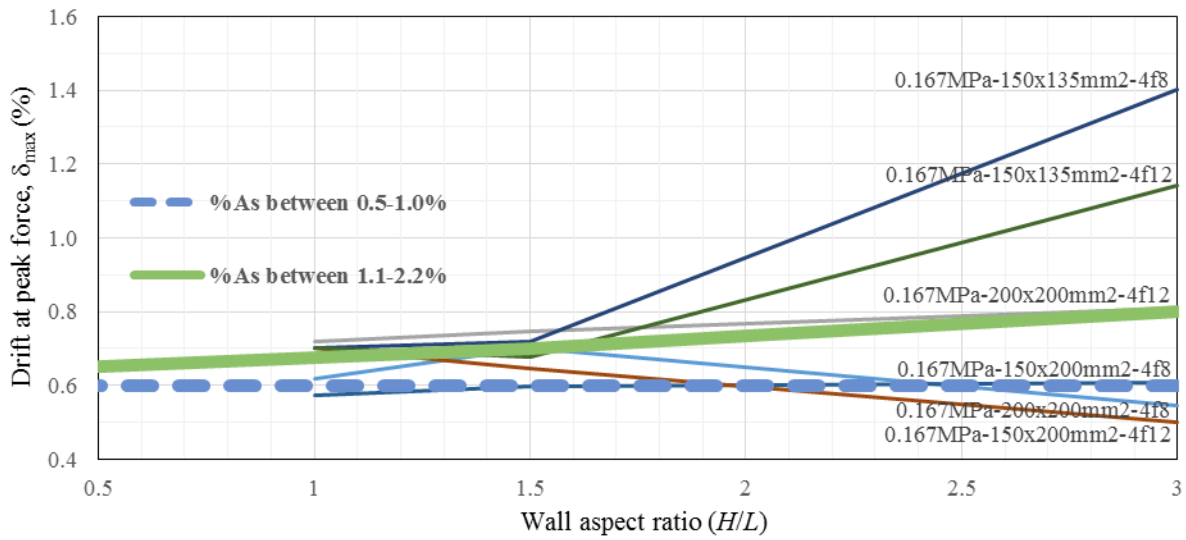

Figure 21. Charts for estimation of δ_{max} for CM walls with a normalized vertical stress $\sigma/f_m = 0.067$

5.3 Force–displacement backbone model

Proposing models for the lateral force–displacement response of CM walls is a step ahead of the simple proposal of formulas for the lateral resistance of the walls. In this regard, a first backbone model to describe the shear failure behaviour of CM walls was proposed by Flores and Alcocer (1996) [39], in which the drift limits were fixed values. Later, Riahi et al. (2009) [35] proposed empirical formulas for both the shear force and displacement characteristics of CM walls to estimate the lateral response according to a trilinear force–displacement backbone model. This last model is applicable to squat CM walls failing by shear, whose behaviour is as described below.

The masonry panel and tie-elements work monolithically, and the wall response is linear elastic at the early stages of loading. Then, the formation of inclined cracks and its progression towards the tie-columns reduce the stiffness of the masonry panel. According to Riahi et al. (2009) [35], the stage at which the first significant diagonal cracking occurs is accompanied by approximately 40% reduction of the panel stiffness (defined as cracking point (δ_{cr}, F_{cr})). After that, the diagonal cracking is extended to the tie-elements and the response is further governed by the behaviour of tie-columns, namely due to dowel action of longitudinal reinforcement (maximum point (δ_{max}, F_{max})). Finally, strength and stiffness degradation occurs due to concrete and masonry crushing, as well as buckling of longitudinal reinforcement in tie-columns, up to the ultimate condition of the wall (ultimate point (δ_{ult}, F_{ult})).

A backbone model with four branches, associated to a very particular shear failure mechanism, has been proposed by Ranjbaran et al. (2012) [13]. Nevertheless, the trilinear model is well accepted in the literature, so it is the one adopted in this work for the shear-dominated failure mechanism. Some authors have proposed changes to the model by Flores and Alcocer (1996) [39], like in Riahi et al. (2009) [35]. In this last study, the following force and drift ratios are proposed: F_{ult}/F_{max} = 0.8 and $\delta_{max}/\delta_{ult}$ = 0.65. A review from the literature of different values for these and similar ratios are listed in Table 5. The adoption of different values for the ratios is related with local variability of test results due to different materials and configurations used for the CM walls, leading to different proportions in the behavioural stages. A more complex formulation of force and drift ratios depending on particular events that drive the failure mechanism are proposed by Yekrangnia (2017) [37].

A CM wall failing by flexure presents a different behaviour, see Varela-Rivera et al. (2019) [3]. In this case, damage starts with horizontal flexural cracks at the bottom part of tie-columns. After, yielding of the longitudinal reinforcement at the bottom end of the tensioned tie-column is reached. Then, as the drift increases, horizontal flexural cracks propagate into the masonry panel and new flexural cracks appear along the height of the tie-columns. This is a much more ductile mechanism, as is evident from the experimental results by Varela-Rivera (2019) [3] and da Porto et al. (2011) [20], and also from the numerical simulations performed in this work. So, a backbone model ending with a horizontal plastic branch and allowing for a larger ultimate drift (e.g. 1% as proposed by Varela-Rivera (2019) [3]), may be more suitable and will be adopted in this work for the flexural-dominated failure mechanism.

There is no study in the literature that explicitly considers different backbone models for the shear and flexural responses of CM walls. An experimental work was developed by Pérez-Gavilán et al. (2015) [2] to assess the response of CM walls with varying *H*/*L*, in order to characterize the stiffness, strength and displacement characteristics of the walls. In turn, a parametric analytical study of CM walls by varying *H*/*L*, the compressive strength of masonry and the vertical stress on the wall, was performed by Erberik et al. (2019) [40]. This last work was based on applying analytical models to support a methodology for seismic performance assessment of CM structures, from the definition of backbone response curves for walls to the parametric assessment of entire buildings. The current work is in the same line, despite it is further based on numerical simulation of CM walls.

From the performed simulations and taken into account the existing studies, a trilinear backbone model is here proposed for both the shear and flexural -dominated responses of CM walls. The assumed force and drift ratios are indicated in Table 5 and the proposed models are exemplified in Figure 22, after correspondence with the pushover curves of given walls among the studied configurations, which are representative of different behavioural proportions. The cracking point is defined to match the numerical capacity curves, with a drift between 0.1 and 0.2 %, and for a lateral force between 50 and 70 % of F_{max}; the ratio F_{cr}/F_{max} may be defined as a function of H/L. The ultimate displacement δ_{ult} is in any case estimated by dividing the drift at the peak force δ_{max} by 0.6. The response of Wall #14 is a midterm between the responses for a shear failure and for a flexural one, like for a combined mechanism, mainly due to the medium reinforcement rate that it presents. The proposed models may in the future be additionally validated against experimental tests of similar walls.

Table 5. Force and drift ratios according to different backbone models

Mechanism / Work	F_{max}/F_{cr}	F_{cr}/F_{max}	F_{ult}/F_{cr}	F_{ult}/F_{max}	δ_{max}	δ_{ult}	$\delta_{max}/\delta_{ult}$
Shear /							
Flores and Alcocer [39]	1.25	-	1.12	0.9	0.003	0.005	0.6
Riahi et al. [35]	-	-	-	0.8	*	*	0.65
Erberik et al. [40]	-	0.7	-	0.8	*	*	-
Proposed	**-**	**0.7**	**-**	**0.8**	***f*(σ, A_s, *H/L*)**	**-**	**0.6**
Flexure /							
Varela-Rivera et al. [3]	§	§	§	§	§	0.01	-
Proposed	**-**	***f*(*H/L*)**	**-**	**1.0**	***f*(σ, A_s, *H/L*)**	**-**	**0.6**

* The ratio is calculated using a formula given in the associated reference work
§ A bilinear equivalent model is assumed based on equating the areas under the envelope and bilinear curves
f(variables) means that the ratio is defined depending on the indicated variables

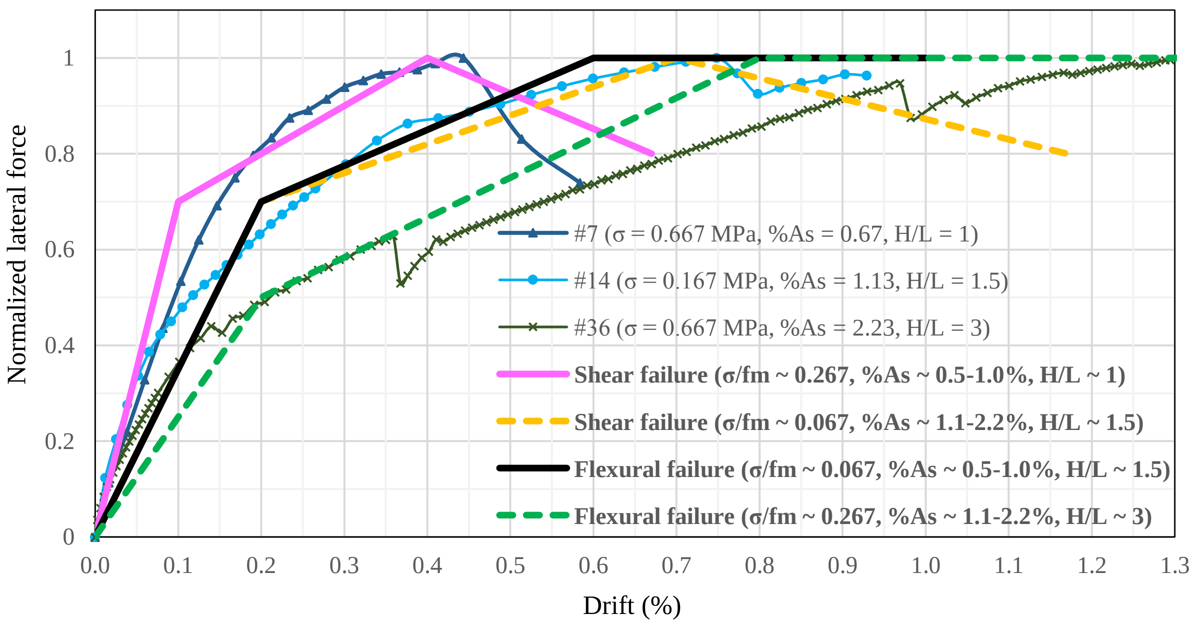

Figure 22. Proposed backbone models after correspondence with pushover curves of given walls

6. Conclusions

The derivation of comprehensive analytical models from numerical simulation results, satisfying the compromise of proposing easy-to-use methods for design, is a major challenge in engineering practice. In this paper, a parametric numerical study of CM walls subjected to lateral in-plane loading and the subsequent proposal of analytical models to characterize the force–displacement response of the walls are presented, towards the definition of backbone models to use in performance-based design. For this purpose, numerical modelling of CM walls has been addressed and a finite element model of a benchmark wall, whose results of testing under lateral in-plane cyclic loading are reported in literature, was developed, including calibration of the mechanical properties of the masonry, RC elements and frame-masonry interface.

From those benchmark experimental tests, it is concluded that the behaviour of CM walls subjected to lateral in-plane loading involves a multipart interaction between the masonry panel and the tie-elements, with both shear and flexural behavioural components. The proportions of these components depend, beyond the material properties, on characteristics like the wall aspect ratio, RC tie-column section and vertical load. Thus, the variation of such characteristics was considered in this work through combination of three values of the wall aspect ratio H/L (1, 1.5, 3), three tie-column sections *Tie-A* (200 x 200 mm^2, 150 x 200 mm^2, 150 x 135 mm^2), two vertical stress levels σ (0.167 MPa, 0.667 MPa) and two longitudinal reinforcement rates in tie-columns A_s (4ϕ8, 4ϕ12), resulting in a set of 36 walls.

Numerical simulation of the push-over loading of each wall was performed and the results were evaluated in terms of lateral resistance, strain and stress patterns, and displacement capacity. Then, based on the obtained results, analytical models have been assessed for estimation of the lateral resistance of CM walls both in shear and flexure. As regards the flexural resistance, a factor may be included in the flexural formula to take into account the efficiency of the reinforcement in tie-columns, i.e. the yield force of reinforcement is multiplied by $(H/L)^{-1/2}$. The better match with the numerical results is obtained when both the shear and flexural strength domains are considered. In given cases, a poor estimation of the lateral resistance is obtained, possibly because a mixed shear-flexural failure occurs. So, a new formulation may be needed to consider it. Charts for estimation of the drift at the peak force are proposed, which are used as input to a trilinear backbone model for both the shear and flexural - dominated responses of CM walls. Because of the limited number of cases investigated (36 walls), the proposed analytical models are mostly applicable to CM walls presenting characteristics, i.e. values of H/L, *Tie-A*, σ and A_s, within the ranges considered in this study.

The presented methodology, from the numerical simulation to the derivation of backbone models for CM walls, can similarly be applied to other structural typologies. This work demonstrates how the application of computational methods, by considering the experimental background and employing engineering judgment, allows to derive suitable analytical models for design. Indeed, the derivation of calculation rules from the experimental testing and/or numerical simulation results is today a major challenge for researchers. The adopted methodology relies on a numerical model which has been calibrated for a particular CM wall scheme, according to the assumed material properties. Furthermore, the proposed backbone models empirically consider the post-peak branch of the response, tailored to the investigated wall configurations. So, the obtained results are mostly applicable to CM walls similar to the benchmark wall and according to the considered configurations. In any case, it is believed that the current work will contribute to a better understanding and design of CM walls.

Declaration of Competing Interests

The authors declare that they have no known competing financial interests or personal relationships that could have appeared to influence the work reported in this paper.

Acknowledgments

The FEM analysis work presented here was developed in the scope of European Commission Mandate ‘M/515 phase 1 tasks for the development of the 2nd generation of EN Eurocodes’ coordinated by the Netherlands Standardization Institute (NEN), task SC6.T1 ‘Masonry - Revised version of EN 1996-1-1’. The prolific discussions and suggestions of participants in the work of PT1 for SC6.T1 are gratefully acknowledged. This work was partly financed by FEDER funds through the Competitivity Factors Operational Programme – COMPETE and by national funds through FCT – Portuguese Foundation for Science and Technology, within ISISE (project UID/ECI/04029/2013). The Postdoc Grant SFRH/BPD/94677/2013 provided to the first author is acknowledged in particular.

Credit Author Statement

Rui Marques: Conceptualization, Methodology, Validation, Formal analysis, Investigation, Data curation, Writing - original draft. **João M. Pereira**: Methodology, Software, Validation, Formal analysis, Writing - review & editing. **Paulo B. Lourenço**: Conceptualization, Validation, Supervision, Project administration.

References

[1] Meli R, Brzev S, Astroza M, Boen T, Crisafulli F, Dai J et al. Seismic design guide for low-rise confined masonry buildings. Oakland: Earthquake Engineering Research Institute (EERI); 2011.

[2] Pérez-Gavilán JJ, Flores LE, Alcocer SM. An experimental study of confined masonry walls with varying aspect ratios. Earthquake Spectra 2015;31(2):945–68. https://doi.org/10.1193/090712EQS284M

[3] Varela-Rivera J, Fernandez-Baqueiro L, Gamboa-Villegas J, Prieto-Coyoc A, Moreno-Herrera J. Flexural behavior of confined masonry walls subjected to in-plane lateral loads. Earthquake Spectra 2019;35(1):405–422. https://doi.org/10.1193/112017EQS239M

[4] Marques R, Lourenço PB. Structural behaviour and design rules of confined masonry walls: review and proposals. Construction and Building Materials 2019;217:137–155. https://doi.org/10.1016/j.conbuildmat.2019.04.266

[5] Janaraj T, Dhanasekar M. Design expressions for the in-plane shear capacity of confined masonry shear walls containing squat panels. J Struct Eng-ASCE 2015;142(2):04015127. https://doi.org/10.1061/(ASCE)ST.1943-541X.0001403

[6] Tripathy D, Singhal V. Estimation of in-plane shear capacity of confined masonry walls with and without openings using strut-and-tie analysis. Engineering Structures 2019;188:290–304. https://doi.org/10.1016/j.engstruct.2019.03.002

[7] Zabala F, Bustos JL, Masanet A, Santalucía J. Experimental behavior of masonry structural walls used in Argentina. In: Proceedings of the 13th world conference on earthquake engineering. Vancouver: Canadian Association for Earthquake Engineering; 2004, paper no. 1093.

[8] Tomaževič M. Earthquake-resistant design of masonry buildings. In: Series on innovation in structures and construction. London: Imperial College Press; 1999.

[9] Uva G, Porco F, Fiore A. Appraisal of masonry infill walls effect in the seismic response of RC framed buildings: a case study. Engineering Structures 2012;34:514–26. https://doi.org/10.1016/j.engstruct.2011.08.043

[10] Pari PDA. Comparación del comportamiento a carga lateral cíclica de un muro confinado con ladrillos de concreto y otro con ladrillos de arcilla. Tesis para optar el Título de Ingeniera Civil. Lima: Pontificia Universidad Católica del Perú; 2008 [in Spanish].

[11] Caliò I, Marletta M, Pantò B. A new discrete element model for the evaluation of the seismic behaviour of unreinforced masonry buildings. Engineering Structures 2012;40:327–38. https://doi.org/10.1016/j.engstruct.2012.02.039

[12] Calderini C, Cattari S, Lagomarsino S. Numerical investigations on the seismic behaviour of confined masonry walls. In: Proceedings of the seismic engineering conference commemorating the 1908 Messina and Reggio Calabria earthquake. Maryland: AIP Publishing; 2008, p. 816–23. https://doi.org/10.1063/1.2963918

[13] Ranjbaran F, Hosseini M, Soltani M. Simplified formulation for modeling the nonlinear behavior of confined masonry walls in seismic analysis. Int J Archit Herit 2012;6(3):259–89. https://doi.org/10.1080/15583058.2010.528826

[14] Eshghi S, Pourazin K. In-plane behavior of confined masonry walls – with and without opening. International Journal of Civil Engineering 2009;7(1):49–60.

[15] Janaraj T, Dhanasekar M. Finite element analysis of the in-plane shear behaviour of masonry panels confined with reinforced grouted cores. Construction and Building Materials 2014;65:495–506. https://doi.org/10.1016/j.conbuildmat.2014.04.133

[16] Smoljanović H, Živaljić N, Nikolić Z, Munjiza A. Numerical model for confined masonry structures based on finite discrete element method. International Journal for Engineering Modelling 2017;30(1-4):19–35.

[17] Medeiros P, Vasconcelos G, Lourenço PB, Gouveia J. Numerical modelling of nonconfined and confined masonry walls. Construction and Building Materials 2013;41:968–76. https://doi.org/10.1016/j.conbuildmat.2012.07.013

[18] Okail H, Abdelrahman A, Abdelkhalik A, Metwaly M. Experimental and analytical investigation of the lateral load response of confined masonry walls. HBRC Journal 2016;12(1):33–46. https://doi.org/10.1016/j.hbrcj.2014.09.004

[19] INPRES-CIRSOC 103, Normas Argentinas para construcciones sismorresistentes, Parte III: Construcciones de mampostería (Argentinean masonry code). Buenos Aires: Ministerio del Interior, Obras Públicas y Vivienda; 1991.

[20] da Porto F, Mosele F, Modena C. In-plane cyclic behaviour of a new reinforced masonry system: experimental results. Eng Struct 2011;33(9):2584–96. https://doi.org/10.1016/j.engstruct.2011.05.003

[21] Gouveia JP, Lourenço PB. Masonry shear walls subjected to cyclic loading: influence of confinement and horizontal reinforcement. In: Proceedings of the 10th North American masonry conference. St. Louis, Missouri: The Masonry Society; 2007, p. 838–48.

[22] DIANA. User's manual of DIsplacement ANAlyzer finite element software package, release 10.2. DIANA FEA, Delft, https://dianafea.com/manuals/d102/Diana.html; 2017 [accessed December 2019].

[23] Selby RG, Vecchio FJ. Three-dimensional constitutive relations for reinforced concrete. Technical Report 93-02. Toronto: University of Toronto, Department of Civil Engineering; 1993.

[24] Rots JG. Computational modelling of concrete fracture. Doctoral thesis. Delft: Delft University of Technology; 1998 [avail. at http://resolver.tudelft.nl/uuid:06985d0d-1230-4a08-924a-2553a171f08f].

[25] INTI-CIRSOC 201. Reglamento Argentino de estructuras de hormigón (Argentinean code for concrete structures). Buenos Aires: Instituto Nacional de Tecnología Industrial; 2005.

[26] EN 1992-1-1. Eurocode 2: Design of concrete structures - Part 1-1: General rules and rules for buildings. Brussels: European Committee for Standardization; 2004.

[27] fib. fib Model Code for Concrete Structures 2010. fédération internationale du béton (International Federation for Structural Concrete). Berlin: Wilhelm Ernst & Sohn; 2013.

[28] Mojsilović N. Strength of masonry subjected to in-plane loading: A contribution. International Journal of Solids and Structures 2011:48(6):865–73. https://doi.org/10.1016/j.ijsolstr.2010.11.019

[29] Angelillo M, Lourenço PB, Milani G. Masonry behaviour and modelling. In: Angelillo M. (ed.) Mechanics of Masonry Structures. CISM International Centre for Mechanical Sciences, vol. 551. Vienna: Springer; 2014. https://doi.org/10.1007/978-3-7091-1774-3_1

[30] Sánchez-Tizapa S. Experimental and numerical study of confined masonry walls under in-plane loads: case: Guerrero State (Mexico). Doctoral thesis. Paris: Université Paris-Est; 2009 [available at https://tel.archives-ouvertes.fr/tel-00537380/file/58_SANCHEZ_Tizapa.pdf].

[31] EN 1996-1-1. Eurocode 6: Design of masonry structures - Part 1-1: General rules for reinforced and unreinforced masonry structures. Brussels: European Committee for Standardization; 2005.

[32] Tomaževič M, Klemenc I. Seismic behaviour of confined masonry walls. Earthquake Engng Struct Dyn 1997;26(10):1059–71. https://doi.org/10.1002/(SICI)1096-9845(199710)26:10<1059::AID-EQE694>3.0.CO;2-M

[33] Priestley MJN, Calvi GM, Kowaisky MJ. Displacement-based seismic design of structures. Pavia: IUSS Press; 2007.

[34] Marques R, Lourenço PB. A model for pushover analysis of confined masonry structures: implementation and validation. Bull Earthquake Eng 2013;11(6):2133–50. https://doi.org/10.1007/s10518-013-9497-5

[35] Riahi Z, Elwood KJ, Alcocer SM. Backbone model for confined masonry walls for performance-based seismic design. J Struct Eng-ASCE 2009;135(6):644–54. https://doi.org/10.1061/(ASCE)ST.1943-541X.0000012

[36] Petry S, Beyer K. Force–displacement response of in-plane-loaded URM walls with a dominating flexural mode. Earthquake Engng Struct Dyn 2015;44:2551–73. https://doi.org/10.1002/eqe.2597

[37] Yekrangnia M, Bakhshi A, Ghannad MA. Force-displacement model for solid confined masonry walls with shear-dominated failure mode. Earthquake Engng Struct Dyn 2017; 46:2209–34. https://doi.org/10.1002/eqe.2902

[38] Turgay T, Durmus MC, Binici B, Ozcebe G. Evaluation of the predictive models for stiffness, strength, and deformation capacity of RC frames with masonry infill walls. J Struct Eng-ASCE 2014;140(10):06014003. https://doi.org/10.1061/(ASCE)ST.1943-541X.0001069

[39] Flores L, Alcocer SM. Calculated response of confined masonry structures. In: Proceedings of the 11th world conference on earthquake engineering. Acapulco: Elsevier Science; 1996, paper no. 1830.

[40] Erberik MA, Citiloglu C, Erkoseoglu D. Seismic performance assessment of confined masonry construction at component and structure levels. Bull Earthquake Eng 2018;17(2):867–89. https://doi.org/10.1007/s10518-018-0468-8